Journal of the North for Basic and Applied Sciences

Peer-Reviewed Scientific Journal

Northern Border University
www.nbu.edu.sa

جامعة الحدود الشمالية
NORTHERN BORDER UNIVERSITY

2007 - ١٤٢٨

IN THE NAME OF ALLAH

THE MOST GRACIOUS, THE MOST MERCIFUL

2007 - 1428
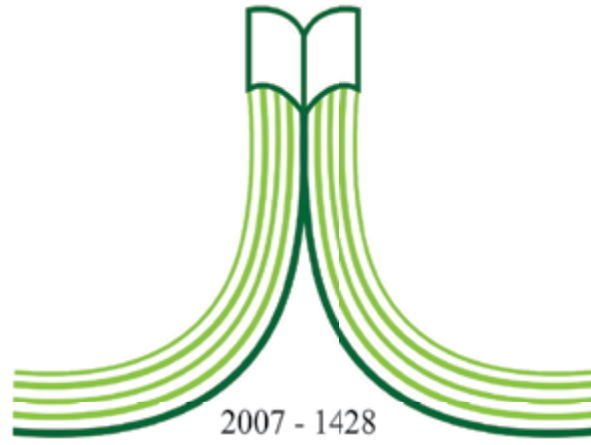
جامعة الحدود الشمالية

NORTHERN BORDER UNIVERSITY

Kingdom of Saudi Arabia

Journal of the North for Basic and Applied Sciences (JNBAS)

Peer-Reviewed Scientific Journal

Journal of the North for Basic and Applied Sciences (JNBAS)

About the Journal

The Journal of the North is concerned with the publication of original, genuine scholarly studies and researches in Basic and Applied Sciences in Arabic and English. It publishes original papers, review papers, book reviews and translations, abstracts of dissertations, reports of conferences and academic symposia. It is a biannual publication (May and November).

Vision

The journal seeks to achieve leadership in the publication of refereed scientific papers and rank among the world's most renowned scientific periodicals.

Mission

The mission of the journal is to publish refereed scientific researches in the field of Basic & Applied Sciences according to well-defined international standards.

Objectives

1. Serve as a scholarly academic reference for researchers in the field of Basic & Applied Sciences.
2. Meet the needs of researchers, publish their scientific contributions and highlight their efforts at the local, regional and international levels.
3. Participate in building a knowledge community through the publication of research that contributes to the development of society.
4. Cover the refereed works of scientific conferences.

Terms of Submission

1. Originality, innovation, and soundness of both research methodology and orientation.
2. Sticking to the established research approaches, tools and methodologies in the respective discipline.
3. Accurate documentation.
4. Language accuracy.
5. The contribution must be unpublished or not submitted for publication elsewhere.
6. The research extracted from a thesis/dissertation must be unpublished or not submitted for publishing elsewhere and the researcher must indicate that the research submitted for publishing in the journal is extracted from a thesis/dissertation.

PUBLICATION INSTRUCTIONS FOR AUTHORS

Submission Guidelines

1. Manuscript must not exceed 35 pages of plain paper (A4).

2. Manuscript must have a title and an abstract in both Arabic and English on one page; the abstract should not be more than 250 words. The manuscript should include, in both languages, keywords that indicate the field of specialization. The keywords are written below each summary and should not be more than six.

3. The author(s) name(s), affiliation(s) and address(es) must be written immediately below the title of the article, in Arabic and English.

4. The Arabic manuscript is typed in Simplified Arabic, in 14-font size for the main text, and 12-font size for notes.

5. The English manuscript is typed in Times New Roman, in 12- font size for the main text, and 9-font size for notes.

6. The manuscript is typed only on one side of the sheet, and line spacing should be single. Margins should be 2.5 cm (or 1.00 inches) on all four sides of the page.

7. The manuscript must have the following organization:

   Introduction: It should indicate the topic and aims of the research paper, and be consistent with its ideas, information and the established facts. The research problem(s) and importance of the literature review should also be introduced.

   Body: The manuscript body includes all necessary and basic details of research approach, tools and methods. All stated information should be arranged according to priority.

   Findings and Discussion: Research findings should be clear and brief, and the significance of these findings should be elucidated without repetition.

   Conclusion: It is a brief summary of the research topic, findings, recommendations and suggestions.

8. Figures, diagrams and illustrations should be included in the main text and consecutively numbered and given titles, with explanatory notes beneath them.

9. Tables should also be included in the main text, consecutively numbered and given titles at the top, with explanatory notes below.

10. Footnotes should be added at the bottom of each page, when necessary. They are to be indicated by numbers or asterisks, in 12-font size for Arabic and 9-font size for English.

11. The Journal of the North does not publish research and measurement tools (instruments). However, they must be included in the submission(s).

12. Citations must follow the American Psychological Association (APA) reference style in which both the author's name and year of publishing are mentioned in the main text, i.e. (name, year). Numbering the references inside the main text and adding footnotes are not allowed.

   Researchers' documentation must be as follows:

   - For single author, the author's family name, followed by a comma, and the publishing year, such as (Khayri, 1985). Page numbers are indicated in the main text in case of quotations, such as (Khayri, 1985, p. 33).

   - If a manuscript has two authors, they must both be cited as shown previously, e.g. (AL-Qahtani & AL-Adnani, 1426 H).

   - If there are multiple (more than two) authors, their family names must be mentioned the first time only, e.g. (Zahran, Al-Shihri, & Al-Dusari, 1995); if the researcher is quoting the same work several times, the family name of the first author followed by *"et al."*[for papers in English] and by "وآخرون" [for papers in Arabic] must be used, e.g. (Zahran *et al.*, 1995) / (1995 ،زهران وآخرون) Full publishing data must be mentioned in the bibliography.

13. Hadith documentation must follow the following example: (Sahih Al-Bukhari, vol.1, p.5, hadith number 511).

14. The bibliography, list of all the sources used in the process of researching, must be added in alphabetical order using the author's last name according to the APA reference style (6th edition) in 12-font size for Arabic and 9-font size for English.

   The bibliography should be organized as follows:

   Citation from books:

   Citation from a one-authored book:

   Shotton, M. A. (1989). *Computer education? A study to computer dependency*. London, England: Taylor & Francis.

Citation from a book of more than one author:

Timothy, N., Stepich, D., & James, R. (2014/1434 H) *Instructional technology for teaching and learning.* Riyadh, Kingdom of Suadi Arabia: University of King Saud Publications.

Citation from Periodicals:

Al Nafaa, A. H. (1427 H). Effect of driving off–road on wild vegetation parks: A study in environmental protection, in the center of the Kingdom of Saudi Arabia. *Saudi Journal of Life Sciences, 14*(1), 35-72.

Citation from M.A. or Ph.D. Thesis:

AlQadi, I. A. (1429 H). *Natural Plants in a Coastal Environment between Rassi Tanoura and Elmalouh in the Eastern Region: A Study in Botanical Geography and the Protection of Environment.* Unpublished Ph.D. Dissertation, College of Arts for Girls, Dammam, Kingdom of Suadi Arabia: King Faisal University.

Citation from Internet References:

Citing an online book:

Almazroui, M .R. & Madani, M. F. (2010). *Evaluation of performance in Higher Education Institutions.* Digital Object Identifier (doi:10.xxxx/xxxx-xxxxxxxx-x), or the Hypertext Transfer Protocol (http://www...), or the International Standard Book Number (ISBN: 000-0-00-000000-0) must be mentioned.

Citing an article in a periodical:

Almadani, M. F. (2014). The definition of debate in reaching consensus. *The British Journal of Educational Technology, 11*(6), 225-260. Digital Object Identifier (doi:10.xxxx/xxxx-xxxxxxxx-x) or the Hypertext Transfer Protocol (http://onlinelibrary.wiley.com/journal/10.1111), or the International Standard Serial Number of the journal (ISSN: 1467- 8535) must be mentioned.

15. It is the researcher's responsibility to translate into English the Arabic bibliography.

Example:

الجبر، سليمان. (1991م). تقويم طرق تدريس الجغرافيا ومــدى اختلافها باختلاف خبــرات المدرسين وجنسياتهم وتخصصاتهم في المرحلة المتوسطة بالمملكة العربية السعودية. **مجلة جامعة الملك سعود- العلوم التربوية**، 3(1)، 143-170.

Al-Gabr, S. (1991). The evaluation of geography instruction and the variety of its teaching concerning the experience, nationality, and the field of study in intermediate schools in Kingdom of Saudi Arabia *(in Arabic). Journal of King Saud University- Educational Sciences, 3*(1), 143-170.

16. Numerals should be the original Arabic numbers (0, 1, 2, 3 ...) in the manuscript.

Required Documents

Researchers are required to submit the following:

1. An electronic copy of their submissions in two formats: Microsoft Word Document (WORD) and Portable Document Format (PDF), to be sent to the following email:

<div align="center">

s.journal.nbu@gmail.com

&

s.journal@nbu.edu.sa

</div>

2. The researcher's CV, including his/her full name in Arabic and English, current work address, email, and academic rank.

3. The researcher must fill out and submit the application for publishing in the Journal of the North, along with the Pledge Statement that his/her submission has not been published before or has not been submitted for publishing elsewhere.

NB

1. The submissions received by the Journal of the North will not be returned whether they are published or not.

2. The published papers reflect only the author's points of view.

3. All accepted manuscripts devolve their property to *the Journal of the North for Basic and Applied Sciences (JNBAS).*

CONTENTS

Manuscripts in English Language

Manuscripts in English Language

Performance Assessment of Contact Separation Triboelectric Generators (CS-TEGs) under various contact frequencies and electrode layers.

Ibrahem R. A.
College of Engineering, Jazan University, Jazan, KSA

Abstract: Triboelectric generators (TEGs) are classified as a novel approach for harvesting energy from small-scale mechanical motions. This work is concerned with improving the performance and output energy from contact separation triboelectric generator (CS-TEG) by using different electrodes under variable contact-separation frequencies. Aluminum or Copper layers were proposed as electrodes for PTFE/PVC, PTFE/Kapton, and Kapton/PVC CS – TEGs. Three contact frequencies were applied for the proposed TEGs for each electrode type under the constant contact load and separating distance of 2N and 0.5mm respectively. Aluminum electrodes that were used for Kapton/PVC CS – TEGs under high contact frequency show significantly improved performance of TEG.

Keywords: Triboelectric generators (TEG), friction energy, contact separation mode, PTFE, PVC, and Kapton TEGs.

(*) **Corresponding Author**:
Ibrahem R. A., College of Engineering, Jazan University, Jazan, KSA.
E-mail: ribrahem@jazanu.edu.sa

تأثير المواد المستخدمة في صناعة الاقطاب الموصلة وكذلك معدل الاتصال والانفصال بين الطبقات العازلة علي اداء المولد الكهربي الاحتكاكي

د. رفاعي احمد ابراهيم

كلية الهندسة - جامعة جازان - المملكة العربية السعودية

المستخلص: تتزايد الجهود البحثية والمحاولات التقنية في الآونة الاخيرة للبحث عن مصادر نظيفة ومتجدده للطاقة وذلك للمساهمة في توفير طاقة بديلة امنة بيئيا ومنخفضة التكاليف وايضا تعتمد علي المصادر الطبيعية والموارد البيئية المتاحة. تعتبر المولدات الكهربية الاحتكاكية (Triboelectric Generators "TEGs") – التي تعتمد علي تحويل الشحنات الكهروستاتيكية الناتجة عن احتكاك المواد المختلفة معا الي طاقة كهربية- من التطبيقات الهندسية الحديثة والتي تهدف الي الاستفادة من الحركات البسيطة لتوليد وتجميع الشحنات الكهربية التي يمكن استخدامها في العديد من التطبيقات الصناعية والطبية. تهدف الدراسة الحالية الي تحسين اداء المولد الكهرو احتكاكي الذي يعتمد علي الية الاتصال والانفصال (Contact-Separation TEG) وذلك من خلال استخدام مواد مختلفة في صناعة الاقطاب الموصلة (Electrodes) مثل النحاس والالومنيوم وايضا الطبقات العازلة مثل PVC، PTFE، Kapton بمعدلات مختلفة لعملية الاتصال والانفصال بين اجزاء المولد. لذلك تم تصميم عدد 6 مولدات كهرو احتكاكية وبناء دائرة كهربية لقياس كميات الطاقة الكهربية الناتجة عن كل منها. اظهرت النتائج تحسن ملحوظ في اداء المولدات التي تكونت من استخدام اقطاب الالومنيوم مع طبقات Kapton/PVC تحت معدلات اتصال وانفصال مرتفعة (3Hz) مقارنة بالمولدات الأخرى، مما يعزز التوصية باستخدام هذه المواد في صناعة المولدات الكهرو احتكاكية التي تعتمد في عملها علي الية الاتصال والانفصال مثل قطرات المطر وحركة الاشخاص اليومية علي الطرقات وغيرها من الحركات الميكانيكية البسيطة.

الكلمات المفتاحية: المولدات الكهربية الاحتكاكية TEGs ، طاقة الاحتكاك، ميكانيزم الاتصال والانفصال C-S mode، البوليمرات المولدة للطاقة

(*) للمراسلة:
د. رفاعي احمد ابراهيم، كلية الهندسة- جامعة جازان – المملكة العربية السعودية.
E-mail: ribrahem@jazanu.edu.sa

11

1. INTRODUCTION

In recent years, looking for clean and renewable energies has remarkably increased and occupied scientists' minds and attention. Energy harvesting techniques from small-scale mechanical actions such as human daily motion, raindrops, and low-vibration movements were introduced as a novel energy solution (Nguyen, et al. 2023). With the increasing popularity of portable and efficient electronic devices, like those utilized on the Internet of Things (IoT), the demand for consistent, reliable, and mobile power sources has become a pressing concern (Raj & Steingart 2018; Xu, Song & Han 2021). This has led to the exploration of energy harvesting methods as a feasible solution for powering these types of devices (Zhang et al. 2021). Triboelectric generators (TEGs) are energy harvesting devices (Chu & Majumdar 2012; Maria et al. 2018; Ibrahem 2022) that can convert mechanical energy from various sources into electrical energy using the triboelectric effect. TEGs operate based on the coupling of triboelectric charges and electrostatic induction, which allows them to generate an output voltage and current (Zhou, Wang, Liu & Zhong 2020). TEGs can operate in several fundamental modes (Niu 2013; Niu & Wang 2015); vertical contact-separation mode - in this mode- the two materials in the TEG move vertically relative to each other, creating a contact and separation cycle (Luo, Jianjun, Wang & Zhong. 2020). This mode is typically used in applications where the two materials are fixed to a substrate and experience a periodic mechanical force, such as in footwear or ocean wave energy harvesting (Luo, Gao & Wang, 2021; Wu 2018). The resulting triboelectric charges generated during the contact and separation cycle are collected by *electrodes and used to generate electrical power. The present work is based on the contact-separation mode.*

Lateral sliding mode- in this mode; two materials in the TEG slide laterally relative to each other, generating triboelectric charges through friction. This mode is typically used in applications where the two materials experience a sliding or rubbing motion, such as touchscreens or self-powered sensors. The triboelectric charges are collected by electrodes and used to generate electrical power (Wang et al. 2016).

Single-electrode mode: In this mode, a single electrode is used to collect the triboelectric charges generated by the contact and separation of two materials (Fan et al. 2012). The single-electrode mode is used in applications where only one electrode is accessible, such as in wearable electronics. This mode can also be used to reduce the complexity and cost of TEGs by eliminating the need for multiple electrodes.

Freestanding mode: In this mode, the two materials in the TEG are not fixed to a substrate, allowing them to move freely and generate triboelectric charges through vibrations or other mechanical motions. This mode is typically used in applications where the TEG must be sensitive to small mechanical motions, such as in self-powered sensors or environmental monitoring. The freestanding mode can also be combined with other modes to enhance the performance of TENGs (Wang et al. 2015).

2. EXPERIMENTS WORK

To investigate the performance of a triboelectric generator based on contact separation mode, test samples were designed in the form of a triboelectric generator that consists of different non-conductor layers as well as different electrode layers. The electrode layers that are used for this work are aluminum or copper film in the form of rectangular layer (12mm x 7mm) with a 0.2mm thickness. Three different triboelectric layers were used for this design; Kapton, PTFE, and PVC in a rectangular form (10mm x 5mm) with a 0.5mm thickness. Triboelectric generators based on contact separation mode are shown in Fig.1. Separating distance of 0.5mm between the contact layers allows the electrons that generate from contact between different materials to transfer from one electrode to another. The present design for TEG is also concerned with the frequency of contact and separation between layers, which also affect the amount of output voltage.

To evaluate the TEGs performance based on different electrodes and different nonconductors; electrical circuits were designed using external load with 10 Ω and 16mf capacitance. The output voltage was measured instantaneously through millimeters under three values of contact separation frequencies 1Hz, 2Hz, and 3Hz.
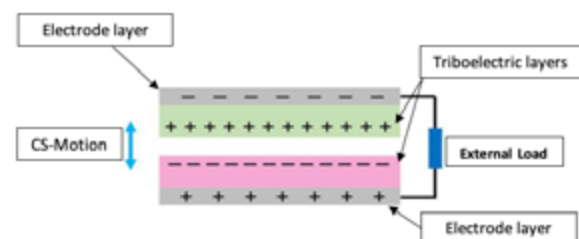

Fig.1 Contact-Separation TEG

3. RESULTS AND DISCUSSION

The triboelectric performance of the proposed contact-separation TEG was investigated through generated voltage. After building Triboelectric generators from the proposed materials for the three models each generator was subjected to repeated press and release of constant load 2N for 60 seconds then the output voltage was measured continuously, each type of CS-TEG was tested three times, and the average result was recorded.

3.1 Effect of aluminum electrodes

Figure 2 shows the output values of the generated voltage on the vertical axis during the time of the test for different contact separation frequencies for CS-TEG that consist of Kapton and PTFE as triboelectric layers and Aluminum Electrode, the average values of the electric voltage from this generator increases with time under high contact-separation frequencies. The output voltage exceeds 104 mV after 30 sec. of the 3Hz contact separation mechanism. The generated voltage for other frequencies also increases with time. In comparison with Figure 3 which explains the effect of using other triboelectric layers (PVC) with Kapton on the same Aluminum electrode; the output voltage increases at high frequencies with time, but the overall performance slightly decreases to 75mV. Figure 4 shows the effect of an aluminum electrode on the generated voltage of PTFE/PVC CS-TEG, the output voltage increases under high frequency to 68mV, low frequencies contact separation shows low values of the generated voltage in comparison with other types of triboelectric layers on the same aluminum electrode.
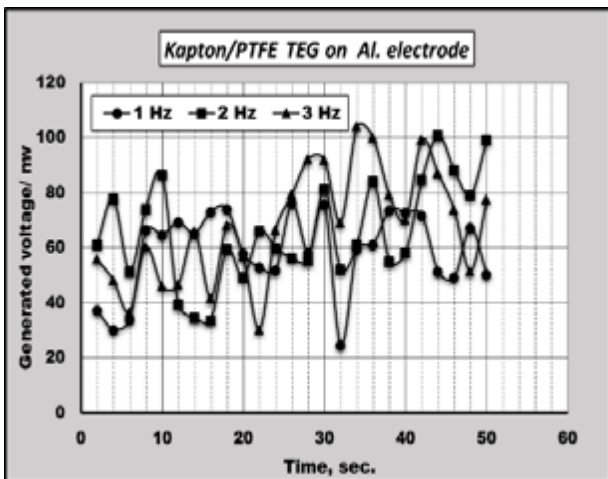

Fig.2 Effect of Al. electrode on the output voltage of Kapton/PTFE CS-TEG

Fig.3 Effect of Al. electrode on the output voltage of Kapton/PVC CS-TEG

Fig.4 Effect of Al. electrode on the output voltage of PTFE/PVC CS-TEG

3.2 Effect of copper electrodes

To obtain the effect of the copper electrode on the generated energy from CS-TEG, a single-layer Kapton/PTFE TEG was tested under different contact separation frequencies. Figure 5 shows that the value of the output voltage slightly increases with time, as well as contact frequency. At a contact separation frequency of 3 Hz, the output voltage was achieved at 43mV after 42 sec. A triboelectric generator that consists of Kapton/PVC dielectric layers on a copper electrode. Figure 6 shows a small rise in voltage compared with Kapton/PTFE CS-TEG on the same electrodes. Figure 7 explains the effect of using PTFE and PVC as triboelectric layers for CS-TEG with copper electrode, as shown in the figure; the generated voltage remains constant between 10 and 25mV for low and medium frequencies, but remarkably increases to 45mV after 50 seconds at high

contact separation frequencies. The overall discussion of the observed results shows that of aluminum electrodes increases the output voltage of CS-TEG in comparison with that of copper electrodes; beside the TEG that consists of Kapton /PTFE dielectric layers shows remarkably improvement of the generated voltage which recommended these TEG to be used for industrial and medical applications (Yuan et al. 2022).
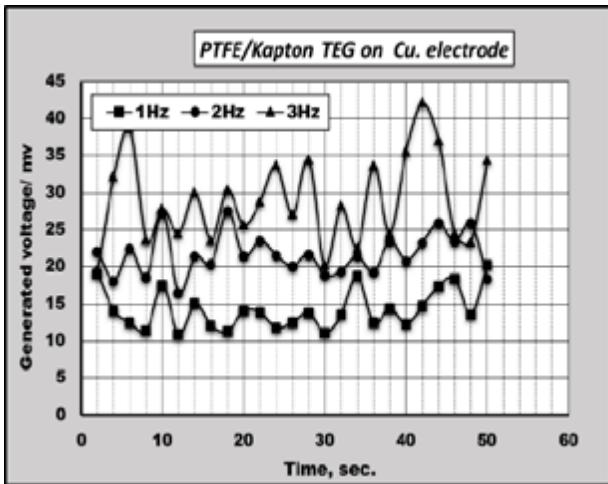
Fig.5 Effect of Cu. electrode on the output voltage of Kapton/PTFE CS-TEG

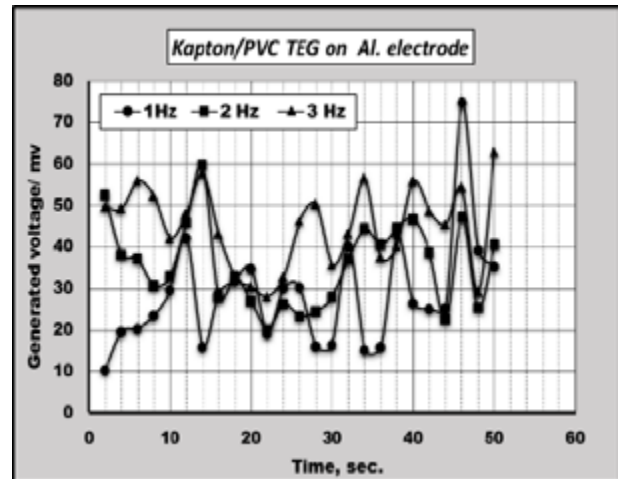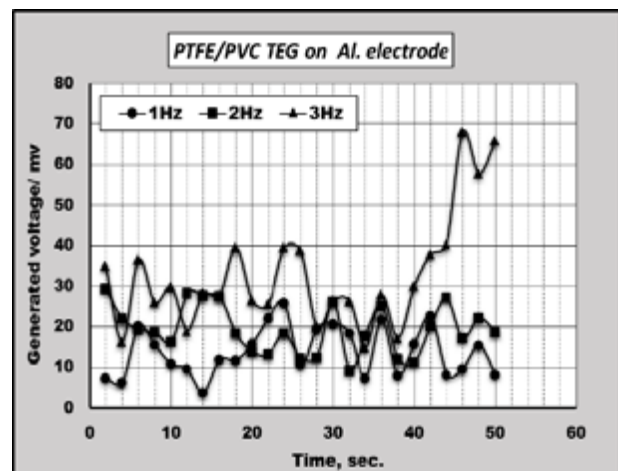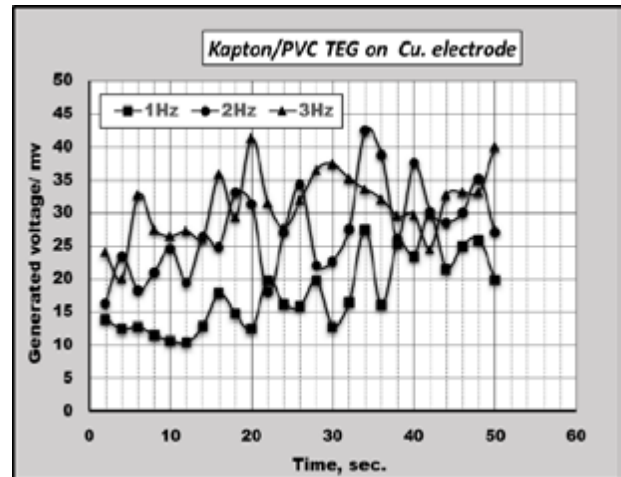**Fig.6 Effect of Cu. electrode on the output voltage of Kapton/PVC CS-TEG**
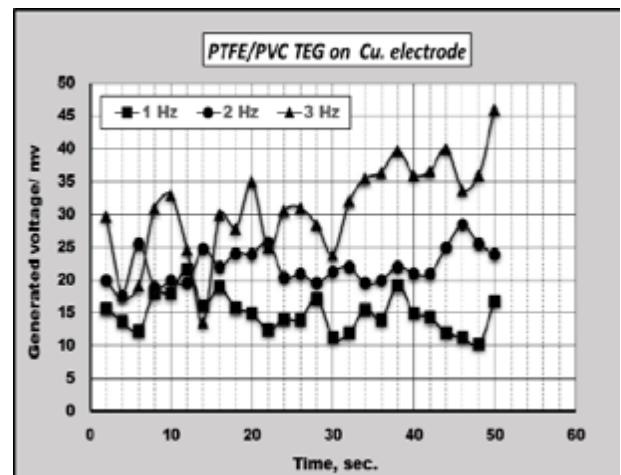
Fig.7 Effect of Cu. electrode on the output voltage of PTFE/ PVC CS-TEG

Table 1: Summary & comparison of the study results

Triboelectric layer for TEG	Cont. Freq. & Electrode Type (mv after 50 sec.)						Max. output
	Low freq. 1Hz		**Med. Freq. 2Hz**		**High freq. 3Hz**		
	AL	Cu	AL	Cu	AL	Cu	
Kapton/PTFE	38	27	40	20	62	40	**62mv.** On Al. under 3Hz
PTFE/PVC	8	24	20	18	65	46	**65mv.** On Al. under 3Hz
Kapton/PVC	45	18	100	20	80	34	**100mv.** On Al. under 2Hz

14

4. CONCLUSION

a. The triboelectric performance of TEG consists of Kapton and PTFE as triboelectric layers significantly enhanced by means of aluminum film as electrodes for electron transfer.

b. TEG that consists of Kapton/PTFE on AL electrodes shows high output values of voltage from 80 to 100 mv under high contact frequency after 50 sec. also, the generated voltage decreases under low contact separation frequency.

c. The use of PTFE/PVC as triboelectric layers for TEG on AL electrodes shows low values of output voltage in comparison with the other types of TEG in this study.

d. Using copper film as an electrode layer for TEGs that consist of Kapton/PTFE triboelectric layers slightly increases the output voltage to 45mv under high contact separation frequencies after 50 sec.

e. For all proposed TEGs the generated voltage increases with an increase in contact separation frequency.

f. It can be recommended that the proposed TEGs be a sustainable source of electrical energy on the roads that afford continuous contact-separation mechanisms.

Future work: a wide range of engineering materials will be proposed as triboelectric layers for different contact mechanisms to enhance the generated energy gained by TEG.

5. References

Chu, S., & Majumdar, A. (2012). Opportunities and challenges for a sustainable energy future. Nature, (488), 294–303.

Fan F. R., Tian Z. Q. & Lin W. Z. (2012). Flexible triboelectric generator. Nano Energy. 1(2), 328-334

Ibrahem R. A., (2022), Triboelectrification performance of carbon fiber reinforced epoxy composites filled with c3n4 nanoparticles, Jouf University Science and Engineering Journal 9 (2), 1-7.

Luo, J. J., Gao, W. C. & Wang, Z. L. (2021). The triboelectric nanogenerator as an innovative technology toward intelligent sports. Advanced Materials, 33(17), 2004178. DOI: 10.1002/adma.202004178

Luo, Jianjun, Wang & Zhong. (2020). Recent progress of triboelectric nanogenerators: From fundamental theory to practical applications. EcoMat. 2. 10.1002/eom2.12059. . https://doi.org/10.1002/ eom2.12059

Maria J. R., Nirmal P., Alluri, N., Vivekananthan, V., Chandrasekhar A., Khandelwal G., & Kim, S. (2018). Sustainable yarn type-piezoelectric energy harvester as an eco-friendly, cost-effective battery-free breath sensor. Journal of Applied Energy, (228), 1767-1776. Doi:10.1016/j.apenergy.2018.07.016.

Nguyen, Q.T., Vu D. L., Le C. D., & Ahn K. K. (2023). Enhancing the Performance of Triboelectric Generator: A Novel Approach Using Solid–Liquid Interface-Treated Foam and Metal Contacts. Polymers (15), 2392. https://doi.org/10.3390/polym15102392

Niu S. & Wang ZL. (2015). Theoretical systems of triboelectric nanogenerators. Nano Energy. (14), 161-192.

Niu, S., (2013). Theoretical study of contact-mode triboelectric nanogenerators as an effective power source. Energy Environ. Sci., (6), 3576–3583.

Raj, A., & Steingart, D. A. (2018). Review—power sources for the internet of things. Journal of the Electrochemical Society, 165(8), 3130-3136. https://doi.org/10.1149/2.0181808jes

Wu, C. S., Wang, A. C., Ding, W. B., Guo, H. Y., & Wang, Z. L. (2018). Triboelectric nano-generator: A foundation of the energy for the new era. Advanced Energy Materials, (9), 1802906. Doi: 10.1002/aenm.201802906

Wang, Zhong & Lin, Long & Niu, Simiao & Zi, Yunlong. (2016). Triboelectric Nanogenerator: Lateral Sliding Mode. 10.1007/978-3-319-40039-6_3.

Xu, C., Song Y.& Han M. (2021). Portable and wearable self-powered systems based on emerging energy harvesting technology. Microsyst Nanoeng. 7(25) https://doi.org/10.1038/s41378-021-00248-z

Yuan Bai, Hongqing Feng, Zhou Li. (2022). Theory and applications of high-voltage triboelectric nanogenerators, Cell Reports Physical Science, 3(11). https://doi.org/10.1016/j.xcrp.2022.101108.

Zhang, S., Xia, Q., Ma, S., Yang W., Wang Q., Yang C., Jin B., & Liu, C. (2021). Current advances and challenges in nanosheet-based wearable power supply devices. Iscience Journal 24(12), 103477 https://doi.org/10.1016/j.isci.2021.103477

Zhou, L., Liu, D., Wang, J., & Zhong W. (2020). Triboelectric nanogenerators: Fundamental physics and potential applications. Friction. (8), doi: 10.1007/s40544-020-0390-3.

Zhu, G., Peng, B., Chen, J., Jing, Q. & Wang, Z. L., (2015). Triboelectric nanogenerators as a new energy technology: from fundamentals, devices, to applications. Nano Energy (14), 126–138.

Adsorption of Cr(VI) onto low-cost activated carbon: isotherm, kinetic and thermodynamic studies

Mohamed Ahmed Mahmoud
Department of Chemical Engineering, College of Engineering, Jazan University, Jazan 45142, Saudi Arabia.

Abstract: The ability of commercial low-cost activated carbon (LC-AC) to adsorb and remove Cr Cr(VI) from the watery system was examined. The batch adsorption procedure investigated various limits for example pH, initial concentration, sorbent dosage, and interaction period. LC-AC was characterized using scanning electron microscopy (SEM). At pH 3.5 and 40 minutes, 6.22 mg/g was the highest adsorption capacity ever recorded. According to kinetic and equilibrium investigations, this process fits a second-order pseudo-model and a Langmuir isotherm. The Van't Hoff equation was utilized to evaluate the temperature-related variables, and the outcomes revealed that the procedure was exothermic. The enthalpy and average adsorption energy (E) values demonstrated that the adhesion action was physical in origin.

(*) **Corresponding Author**:

Mohamed Ahmed Mahmoud, Department of Chemical Engineering, College of Engineering, Jazan University, Saudi Arabia.

Jazan: 11592

E-mail: Momahmoud@jazanu.edu.sa

امتزاز الكروم السداسي على الكربون المنشط منخفض التكلفة: دراسات منحنيات الامتزاز والحركية والديناميكية الحرارية

د. محمد احمد محمود

قسم الهندسة الكيميائية، كلية الهندسة، جامعة جازان، جازان 45142، المملكة العربية السعودية.

مستخلص البحث: تـم فحـص قـدرة الكربـون المنشـط التجـاري منخفـض التكلفـة علـى امتصـاص وإزالـة الكـروم السداسـي مـن النظـام المائـي. عوامـل الامتـزاز الدفعـي المختلفـة مثـل الرقـم الهيدروجينـي، التركيـز الاولـى، وجرعـة المـادة الماصـة، وزمـن التفاعـل تـم التحقـق منهـا. تـم توصيـف الكربـون المنشـط باسـتخدام المجهـر الإلكترونـي الماسـح. عنـد درجـة حموضـة 3.5 و40 دقيقـة، كانـت 6.22 مجم/جـم أعلـى قـدرة امتصـاص تـم تسـجيلها علـى الإطـلاق. وفقـا لدراسـات الحركيـة والاتـزان، فـإن هـذه العمليـة تتناسـب مـع نمـوذج درجـة الحركيـة الرتبـة الثانيـة الزائفـة، ونمـوذج ايزوثيـرم لانجميـر. تـم اسـتخدام معادلـة فانـت هـوف لتقييـم المتغيـرات المرتبطـة بدرجـات الحـرارة، وأظهـرت النتائـج أن عمليـة الامتـزاز طـاردة للحـرارة. أظهـرت قيـم المحتـوى الحـراري ومتوسـط طاقـة الامتـزاز أن عمليـة الامتـزاز فيزيائيـة

كلمات مفتاحية: الامتزاز؛ الحركية؛ الديناميكا الحرارية؛ كربون منشط

(*) للمراسلة:
د. محمد احمد محمود، قسم الهندسة الكيميائية، كلية الهندسة، جامعة جازان، المملكة العربية السعودية.
جازان: 45142
E-mail: ribrahem@jazanu.edu.sa

1. Introduction

Chromium has negative environmental and health implications when used in excess. Before being released into the environment, effluent containing chromium must be treated to reduce contamination and related risks (Thirugnanasambandham and Shine, 2018). Numerous health issues, such as lung cancer, respiratory conditions, and skin irritation, may result from contact with high doses of Cr(VI) through drinking water besides inhalation (Mahmad et al., 2016; Abutaleb et al., 2023). Aquatic animals and ecosystems can be harmed by chromium pollution in water bodies, and sediment can become contaminated. Additionally, it may have an impact on crops and lower agricultural output (Genawi et al., 2020; Yan et al., 2023). Chromium can be eliminated from wastewater using a variety of techniques, including:

- Chemical precipitation (Nwabanne et al., 2018; Min et al., 2023): Chromium precipitates out of solution as an insoluble compound when chemicals like lime or ferrous sulphate are added to the wastewater. This insoluble product can then be removed by settling or filtration (Aoudj et al., 2017).

- Ion exchange (Elabbas et al., 2016): Chromium ions in wastewater can be selectively adsorbed and eliminated using ion exchange resins. The resin can be recycled after becoming fully saturated with chromium.

- Adsorption (Sadeghi et al., 2017; Abutaleb et al., 2021; Patil et al., 2023; Ayman et al., 2022): Through surface interactions, adsorbents like activated carbon or other unique adsorbents can remove chromium ions from wastewater.

- Membrane filtration (Singh et al., 2018): techniques like reverse osmosis and ultrafiltration enable water to flow

- Biological treatment (Ziati et al., 2018; Mubarak et al., 2024): Some microbes, including bacteria and fungi, have the ability to fix or decrease Cr(VI) to the less hazardous Cr(III). Wastewater treatment can make use of this bioreduction.

- Electrocoagulation (Elabbas et al., 2020): In this technique, wastewater is exposed to an electric current, creating a coagulant that makes it easier to remove chromium by flocculation and sedimentation. In this study, activated carbon which is widely available and reasonably priced was used to eradicate Cr(VI) ions from the watery system. This study looked into the abolition of Cr(VI) from liquid feed using common, inexpensive activated carbon. Cr(VI) uptake was investigated using contact time, starting metal ion concentration, pH, sorbent dosage, and temperature during experiments carried out

in a batch system. Investigations were made on the adsorption process's kinetics, isotherms, and thermodynamics.

2. Resources and approaches

2.1 Preparation of adsorbent material

Low-cost activated carbon (LC-AC) obtained as an agricultural byproduct (corn cob) was converted into low-cost adsorbent. At 450°C, the carbonization process took place, whereas the activation process was carried out in the presence of KOH.

2.2 Preparation of Cr (VI) stock solution

Dissolve the specified amount of $K_2Cr_2O_7$ in a watery system and dilute to the necessary attentiveness to produce a base solution containing 1000 mg/l Cr(VI). The chemicals were all AR grade and came from Sigma-Aldrich in Germany. 0.1N of NaOH and HCl were utilized to change the pH.

2.3 Batch experiment

The objective of the batch study is to examine the different conditions under which Cr(VI) adsorbs onto LC-AC. adding Cr(VI) preparations to Erlenmeyer flasks holding LC-AC is the process. Initial concentrations of 10–60 mg/L, pH ranges of 3–8, and variable durations of time at 30–60°C in a thermostatic shaking water bath are the parameters of the experiment. The water bath was shaken at 120 revolutions per minute using a thermostat. A five-minute centrifugation at 5000 rpm came after sample separation and agitation. The remaining Cr(VI) content was determined by a UV spectrophotometer (Perkin Elmer, A 800) at 370 nm. Adsorption capability (q) was defined as:

$$q = \frac{C_p - C_e \times V}{M} \quad (1)$$

Wherever

C_p = primary attentiveness of Cr(VI) (mg/L)

C_e = attentiveness of Cr(VI) at steadiness (mg/L)

V = bulk of Cr(VI) (L)

W = sorbent dosage of (LC-AC) (g)

According to the following equation, the removal percent (Re) is determined:

$$R_e (\%) = \frac{C_p - C_e \times 100}{C_0} \quad (2)$$

Fig. 1 The series of experimentation sequence

18

3. Outcomes and discussion

3.1 LC-AC's characterization

SEM image of LC-AC prior to adsorption is shown in **Fig.2 (a)**. The surface appears to be irregularly shaped, rough, and porous. These features imply that the surface has a wide surface area and numerous fissures, which may enable effective adsorption between Cr(VI) ions and (LC-AC). Roughness and porosity give the Cr(VI) ions plenty of opportunities to interact with (LC-AC), possibly resulting in successful adsorption. The adsorption process may have caused certain alterations in the LC-AC based on the loss of porosity and roughness on the LC-AC surface **(Fig. 2(b))**. The Cr(VI) ions may have formed a connection with the surface, clogging the pores and smoothing out the imperfections. This change can be a sign that the target molecules were successfully adsorbed onto the LC-AC.

The N_2-adsorption/desorption isotherms of LC-AC produced at 450 °C are shown in **Fig. 2(c)**. Based on IUPAC categorization, it indicates that the isotherm curves are most likely type I, indicating that the LC-AC is a microporous material with a surface area of 32.54 (m^2/g) and a pore volume of 0.028 (cm^3/g). There is a large range of pore diameters in materials, as indicated by the lack eyhof a distinct plateau.
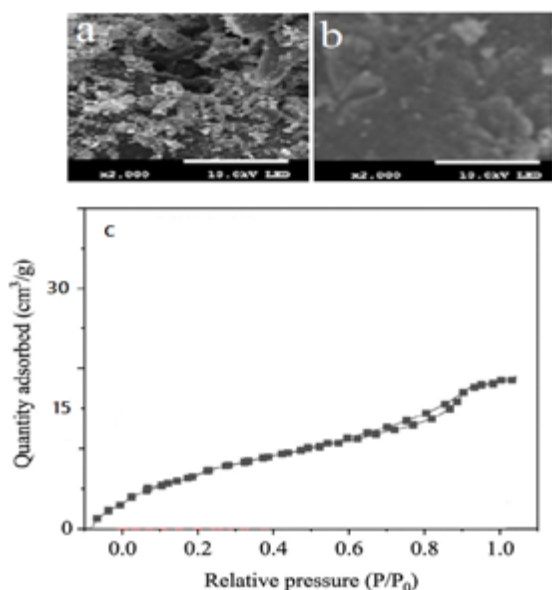
.
Fig. 2 SEM image of Raw LC-AC (a) and Cr(VI) loaded LC-AC (b) N_2 adsorption isotherm for activated carbon (c)

3.2 Adsorption Investigations.

3.2.1 Result of pH:

The role of pH was examined by varying pH values from 3 to 8 at 30°C, 50 mg/l, 0.20 g/50 ml of adsorbent, 120 rpm of agitation, and 60 min **(Fig. 3)**.

The elimination efficiency of ions augmented at pH levels between 3 and 3.5. This indicates that as the pH rose within this range, more Cr(VI) ions were adsorbed onto the (LC-AC) material. At pH 3.5, the maximal capacity for Cr(VI) ions was attained. This shows that the (LC-AC) material had the greatest affinity for Cr(VI) ions at this particular pH. Lower pH levels (below 3.5) occasioned a reduction in the effectiveness of Cr(VI) ion removal. This might be because Cr(VI) ions and H+ ions are vying for the same adsorption sites on the (LC-AC) material. The amount of Cr(VI) ions that might be removed from the solution decreased as a result of this competition (Peng & Guo, 2020). The effectiveness of removing metal was reduced above a pH of 3.5. Hydrolysis, and chemical reaction in which molecules in water are broken down as a result of an increase in hydroxide ions (-OH) when the pH rises, is responsible for this decline in efficiency (Ali Maitlo et al., 2019).
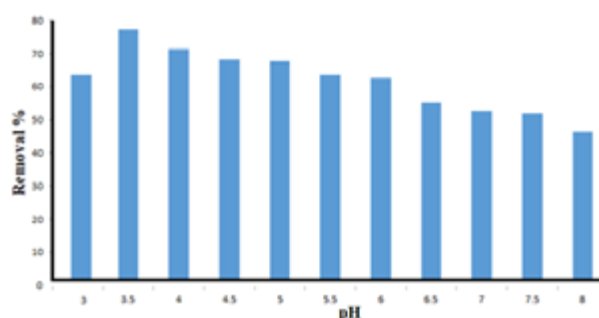
Fig. 3 Efficacy of pH on Cr (VI) ion binding to LC-AC

3.2.2 Effect of contact time:

The interaction period theatres a significant part in deciding how long it takes for the adsorbent (LC-AC) to absorb the greatest amount of the Cr(VI) adsorptive. The uptake procedure has more periods to take place the longer the contact time is. In your case, equilibrium is attained after 40 minutes under the indicated parameters of temperature (30°C), pH (3.5), and adsorbent dose (0.20g). As the contact period lengthens, Cr(VI) ion uptake also grows (Fig. 4). To be sure that the system genuinely reaches equilibrium, additional time may be allowed in some investigations, such as those that determine equilibrium adsorption isotherms. To better understand the uptake procedure, many kinetic replicas are being employed, e.g. pseudo-first-order, pseudo-second-order, Elovich, and intraparticle distribution.
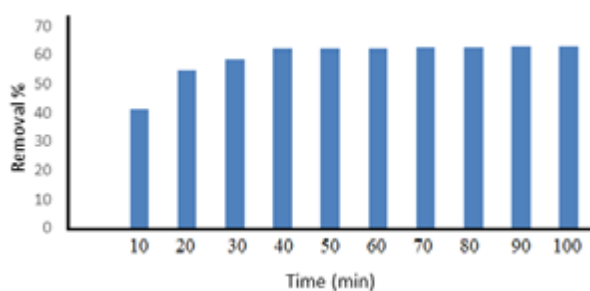
Fig. 4 Efficacy of interaction duration on the Cr (VI) elimination.

19

The pseudo-first-order kinetic model (Prasetyaningrum et al., 2018):

$$\log(q_e - q_t) = \log q_e - \frac{k_1}{2.303} t$$

(3)

The Pseudo-second-order model (Heffron et al., 2016):

$$\frac{t}{q_t} = \frac{1}{k_2 q_e^2} + \frac{1}{q_e} t$$

(4)

The Elovich model (Al-Qodah and Al-Shannag (2017):

$$q_t = \frac{1}{\beta} \ln(\alpha\beta) + \frac{1}{\beta} \ln(t)$$

(5)

The intraparticle diffusion model (Tejada-Tovar et al., 2020):

$$\log R_e = \log K_{id} + a \log(t)$$

(6)

Wherever qe & qt are the adhesion capabilities (mg/g) at stability and at time t, accordingly,, K1 and K2 are the factors of kinetic replicas. β & α are the Elovich coefficients. Kid is the Intraparticle constant. The rate-dependent compatibility of the experiment's results was examined by evaluating the correlation value (R2) (Prasetyaningrum et al., 2018).

$$R^2 = \frac{\sum_{i=1}^{n}(q_{e\ experimental} - q_{e\ theoritical})^2}{\sum_{i=1}^{n}(q_{e\ experimental} - q_{e\ theoritical})^2 + \sum_{i=1}^{n}(q_{e\ experimental} - q_{e\ theoritical})^2}$$

(7)

The larger R2 clearly demonstrated that the Cr(V1) adsorption kinetics closely resemble the pseudo-first-order model, as shown by Table 1 and Fig. 5. As a result, it became clear that physic-adsorption is crucial to the uptake of Cr(V1) by LC-AC (Mahmad et al., 2016).

Table 1. Adsorption kinetic model constants.

Models	Constant	Value
Pseudo-first-order	K1	0.090
	qe	1.666
	r2	0.996
Pseudo-second-order	qe	8.3961
	K2	0.0084
	r2	0.9566
Elovich	β	1.8231
	α	0.7898
	r2	0.9352
Intraparticle distribution	Kid	2.1592
	a	0.4246
	r2	0.8587
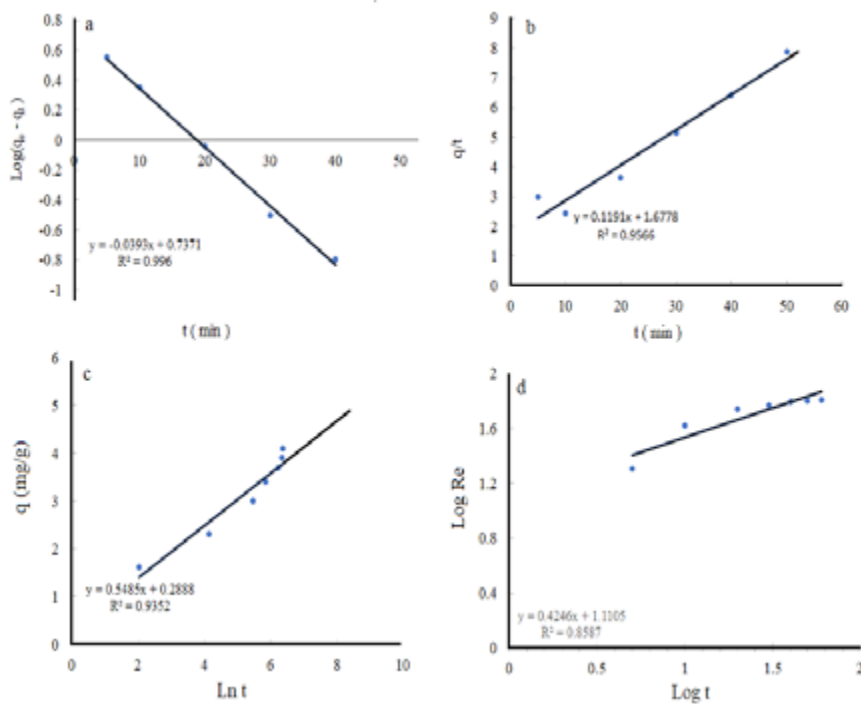
Fig. 5 Pseudo-first order (a) Pseudo-second order (b) Elovich (c) and Intraparticle diffusion (d) models.

20

3.2.3 Result of preliminary Cr(VI) concentrations:

The outcomes demonstrated that the adhesion capabilities rose from 3.32 to 6.22 mg/g as the starting Cr(VI) attentiveness augmented from 10 to 60 mg/L at 30°C, 0.20 g adsorbent dosage, 40 min, and pH 3.5. This indicates that while the starting concentration was higher, the adsorbent was able to trap more Cr(VI) ions. Additionally, the removal effectiveness decreased as the starting Cr(VI) content increased, indicating that the adsorbent was less efficient at eradicating Cr(VI) from the solution at higher preliminary concentrations and the open adsorption sites on the adsorbent became saturated (Khan et al., 2019). This shows that the accessible sites on the adsorbent are filled up as additional Cr(VI) ions are added to the solution, and eventually, no further adsorption can take place due to the adsorbent's limited capacity (He et al., 2020). To make the outcomes of experiments more accurate, the Freundlich isotherm and Langmuir replicas are used. Designing and improving adsorption methods for use in water treatment, pollution management, and other environmental applications requires the use of such data.

The Langmuir isotherm (Pavithra et al., 2020):

$$C_e/q_e = 1/Q_0 b + C_e/Q_0 \tag{8}$$

Where b (L/ mg) and Q0 (mg /g) are Langmuir coefficients.

The rudimentary qualities of the Langmuir faultless can be outlined using the distinction of dynamic RL (Liu et al., 2018).

$$R_L = \frac{1}{1 + b\,C_0} \tag{9}$$

If 0 < RL < 1 implies that the binding mechanism is positive.

The Freundlich isotherm (Das and Nandi, 2020):

$$Log\,q_e = \log(K_f) + 1/n \log(C_e) \tag{10}$$

In which KF and n are Freundlich parameters.

A better fit between the model and the experimental data is shown by higher R2 values (**Table 2**). There is a significant connection between the model and the data when the R^2 value is close to 1. The fact that the R2 value for the Langmuir isotherm is greater (0.983 > 0.921) shows that the Freundlich model does not adequately account for the investigational outcomes and that the Langmuir model does. From this, one can infer that the interaction of Cr(VI) onto LC-AC exists most likely the result of a monolayer adsorption process, as shown by the Langmuir isotherm (**Fig. 6**) (Chouhan et al., 2018).
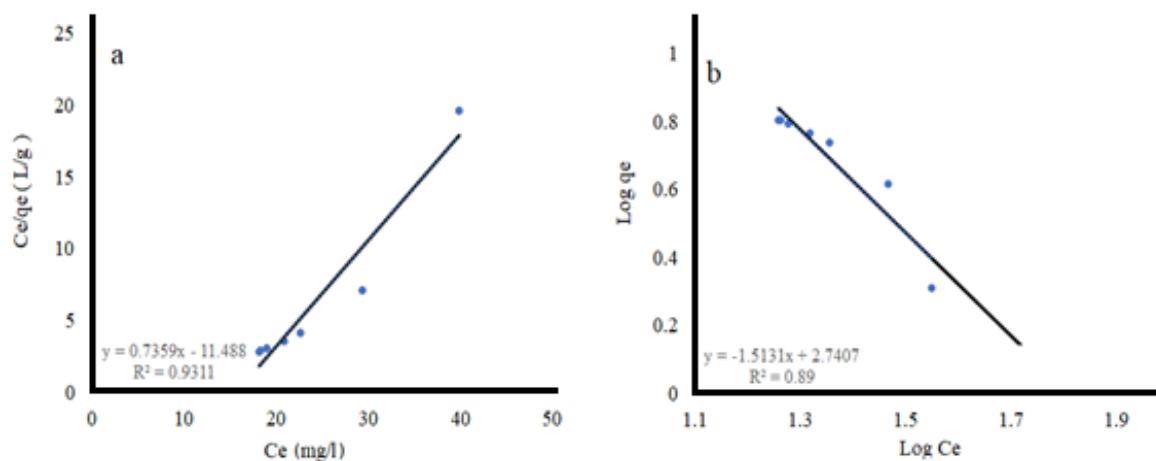

Fig. 6 (a) Langmuir (b) Freundlich isotherms of adsorption of process

Table 2. The adsorption system's Langmuir (a) and Freundlich (b) constants.

Langmuir				Freundlich		
b	Q0	RL	r2	Kf	n	r2
0.0640	1.358	0.6095	0.9311	6.6839	6.6608	0.890

3.2.4   Effect of adsorbent dose:

LC-AC was used in the experiment at different doses (0.01- 0.26g) for 40 minutes, pH 3.5 and 30°C. The elimination efficiency of Cr(VI) rose when the adsorbent dose augmented beginning 0.01g to 0.18g, as shown in Fig. 7. The attendance of extra energetic locations on the LC-AC may be due to the improvement in removal effectiveness with increasing adsorbent dosages. More adsorbent means more active sites for the Cr(VI) ions to bind to and be drawn out of the solution.

This is probably because bigger doses of the adsorbent have an increased surface area (Martín-Domínguez et al., 2018). However, subsequent increases in adsorbent dosage did not lead to a corresponding improvement in removal efficiency after a certain point (particularly when the adsorbent dose climbed beyond 0.18g). This shows that there is a limit to the benefits. At this point, the number of adsorbent particles may cause the adsorption sites to become congested, which could cause certain adsorption sites to overlap or become inaccessible (Emamjomeh et al., 2017).
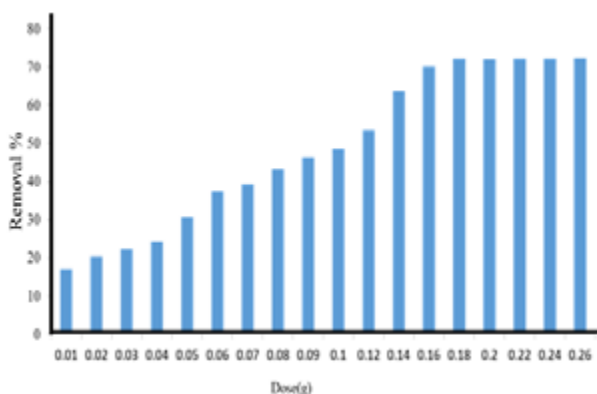

Fig. 7 The significance of LC-AC dosage on Cr(VI) removal.

3.3   Thermodynamic Studies

The temperature's effect on the Cr(VI) uptake was examined amid 30 and 60°C.As the temperature rose, It became apparent that eliminating Cr(VI) ions was less effective. The following equations (Babakhouya et al., 2019) were used to estimate the factors enthalpy ($\Delta H°$), entropy ($\Delta S°$), and Gibbs free energy ($\Delta G°$), using the diffusion coefficient (KD).

$$LnK_D = \frac{\Delta S°}{R} - \frac{\Delta H°}{RT} \tag{16}$$

$$K_D = \frac{q-}{Ce} \tag{17}$$

$$\Delta G° = \Delta H° - T \Delta S° \tag{18}$$

Table 3 shows that the -ve of $\Delta H°$ demonstrates that the adsorption procedure is exothermic. Also, the assessment of $\Delta H°$ can reveal information on the kind of adsorption (**Fig.8**) (Kim et al., 2020). The two primary categories are physical (physisorption) and chemical (chemisorption). In contrast to chemisorption, which typically involves greater heats of adsorption (80–200 kJ/mol), physical adsorption typically involves relatively lower heats of adsorption (2.1-20.9 kJ/mol) (Peng et al., 2019). Given that $\Delta H°$ has an absolute value of -5.278 kJ/mol (Table 4), The binding of Cr(VI) by LC-AC is most likely a physical sorption mechanism involving both types of elements. The minus sign of $\Delta G°$ demonstrates the potential and spontaneity of the act of adsorption, which means that the adsorption will take place naturally without the need for outside energy. During the solid/solution interface, a negative $\Delta S°$ denotes a reduction in unpredictability (Aboulhassan et al., 2018).

Table 3: Temperature-dependent thermodynamic variables.

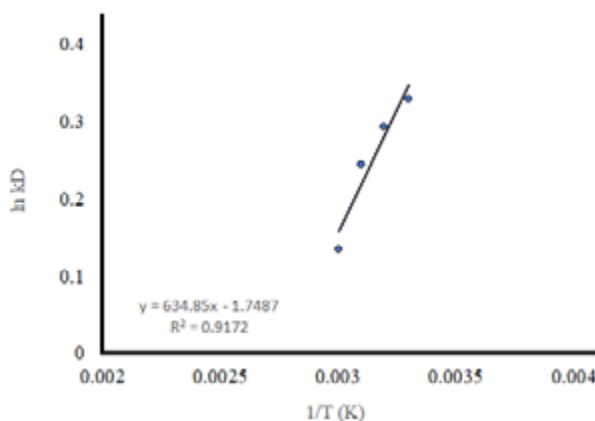| $\Delta H°$ (kJ/mol)	$\Delta S°$ (KJ/mol.K)	$\Delta G°$(kJ/mol)			
		30°C	40°C	50°C	60°C
-5.278	-0.0145	-0.8845	-0.7395	-0.5945	-0.4495

Fig. 8   ln KD vs 1/T(K) Van't Hoff conspiracy.

The energy change brought about by the transmission of a single mole of a sorbate species starting an infinitely diluted solution to the surface of a material is referred to as the mean free energy (E) of sorption. It offers an understanding of how the adsorbate and adsorbent surfaces interact using the following equations (Mamelkina et al., 2019).

$$E = RTLnK_D \qquad (16)$$

wherein R is the ideal gas standard (8.314 J/(mol. K)). The amount of mean free energy is able to reveal information about how strongly the adsorbate interacts with the adsorbent surface. Because temperature can affect the interactions between adsorbate and adsorbent, the mean free energy values varied with temperature. The binding mechanism is physical if E is less than 8 kJ/mol; otherwise, it is chemical. Where E exceeds 8 kJ/mol (Petrie et al., 2015). According to Table 4, as the temperature fluctuated between 30°C and 60°C, the mean free energy (E) changed from 2.799 to 5.559KJ/mol, respectively. The mean free energy values suggest that the physical-binding mechanism supported the results obtained by ΔH° value.

Table 4: Free Energy (E) at various temperatures.

Temperature °C	q (mg/g)	KD	E(KJ/mol)
30	6.22	0.329101	2.799
40	6.00	0.293399	3.19
50	5.45	0.243957	3.788
60	4.22	0.134181	5.559

4. Conclusions

This study's investigation of LC-AC revealed that it has good potential for purging water-based solutions of Cr(VI). At pH 3.5 and 40 minutes of contact time, the highest ability to adsorb (qe) ever recorded was 6.22 mg/g. The results of the kinetic and equilibrium analyses indicate that the procedure of binding matches the pseudo-second-order and the Langmuir isotherm. The uptake method is instantaneous and exothermic in nature. The LC-AC's binding of Cr(VI) is physical in nature, according to the estimated values of ΔH° and sorption energy (E).

5. Conflict of Interest

The authors have declared no conflict of interest

6. References

Aboulhassan, M. A., El Ouarghi, H., Ait Benichou, S., Ait Boughrous, A., & Khalil, F. (2018). *Influence of experimental parameters in the treatment of tannery wastewater by electrocoagulation Separation Science and Technology (Philadelphia), 53(17), 2717-2726.*

Abutaleb, A., Mohd, I., Nasser, Z., Afzal, H. K., Shahir, H., Mohammad, A. A., Omer, B., Mohammad, A. G., Nadeem, A. K., Hitesh, P., Sasan, Z. (2023). *Fe3O4-multiwalled carbon nanotubes-bentonite as adsorbent for removal of methylene blue from aqueous solutions. Chemosphere 316,137824.*

Abutaleb, A., Mubarak, A. E., Mohd, I., Kamal, K. T., Omer Y. B., Nasser, Z., Salah, E. F. H., Mohamed, H. (2021). *Active adsorption performance of planetary ball milled Saudi Arabian bentonite clay for the removal of copper ions from aqueous solution Europhysics Letters 135 (3), 30005.*

Al-Qodah, Z. & Al-Shannag, M. (2017). *Heavy metal ions removal from wastewater using electrocoagulation processes: A comprehensive review Separation Science and Technology (Philadelphia), 52(17), 2649-2676.*

Ali Maitlo, H., Kim, K. H., Yang Park, J., & Hwan Kim, J. (2019). *Removal mechanism for chromium (VI) in groundwater with cost-effective iron-air fuel cell electrocoagulation Separation and Purification Technology, 213, 378-388.*

Aoudj, S., Cheknane, B., Zemmouri, H., Zermane, F., Khelifa, A., Hecini, M., & Drouiche, N. (2017). *Kinetics and adsorption isotherm for the removal of fluoride and chromium (VI) from wastewater by electrocoagulation Desalination and Water Treatment, 82, 262-270.*

Ayman, Y., Ahmed, F.F. A., Nasser, Z., Mohamed, H., Mubarak, A. E., Haitham, M. H., Sahar, S., Ibrahim, M. M. (2022). *The Enhanced Electrosorption Capacity of Activated Charcoal (AC) and WC@AC Composite for Water Desalination through Capacitive Deionization. Int. J. Electrochem. Sci., 17,22108.*

Babakhouya, N., Abdouni, M., & Louhab, K. (2019). *Electrochemical chromium(VI) recovery process by conducting composite, Olive Pomace/Pani Revue Roumaine de Chimie, 64(9), 747-753.*

Chouhan, A., Thakur, L. S., Patidar, K., & Varma, A. K. (2018). *A Review on Removal of Heavy Metals from Water / Wastewater by Electrocoagulation Process. International Research Journal of Engineering and Technology (IRJET), 5(12), 934-944.*

Das, D. & Nandi, B. K. (2020). *Removal of Hexavalent Chromium from Wastewater by Electrocoagulation (EC): Parametric Evaluation, Kinetic Study and Operating Cost. Transactions of the Indian Institute of Metals, 73, 2053-2060.*

Elabbas, S., Ouazzani, N., Mandi, L., Berrekhis, F., Perdicakis, M., Pontvianne, S., Pons, M. N., Lapicque, F., & Leclerc, J. P. (2016). *Treatment of highly concentrated tannery wastewater using electrocoagulation: Influence of the quality of aluminium used for the electrode Journal of Hazardous Materials, 319, 69-77.*

Elabbas, S., Adjeroud, N., Mandi, L., Berrekhis, F., Pons, M. N., Leclerc, J. P., & Ouazzani, N. (2020). *Eggshell adsorption process coupled with electrocoagulation for improvement of chromium removal from tanning wastewater. International Journal of Environmental Analytical Chemistry. Advance online publication. https://doi.org/10.1080/03067319.2020.1761963*

Emamjomeh, M. M., Jamali, H. A., & Moradnia, M. (2017). *Optimization of nitrate removal efficiency and energy consumption using a batch monopolar electrocoagulation: Prediction by RSM method. Journal of Environmental Engineering, 143(7), 04017022.*

Genawi, N. M., Ibrahim, M. H., El-Naas, M. H., & Alshaik, A. E. (2020). *Chromium removal from tannery wastewater by electrocoagulation: Optimization and sludge characterization. Water, 12(5), 1374.*

He, C., Gu, L., Xu, Z., He, H., Fu, G., Han, F., Huang, B., & Pan, X. (2020). *Cleaning chromium pollution in aquatic environments by bioremediation, photocatalytic remediation, electrochemical remediation and coupled remediation systems. Environmental Chemistry Letters, 18(3), 561-576. https://doi.org/10.1007/s10311-019-00960-3*

Heffron, J., Marhefke, M., & Mayer, B. K. (2016). *Removal of trace metal contaminants from potable water by electrocoagulation. Scientific Reports, 6, 28478.*

Khan, S. U., Islam, D. T., Farooqi, I. H., Ayub, S., & Basheer, F. (2019). *Hexavalent chromium removal in an electrocoagulation column reactor: Process optimization using CCD, adsorption kinetics and pH modulated sludge formation. Process Safety and Environmental Protection, 122, 118-130.*

Kim, T., Kim, T. K., & Zoh, K. D. (2020). *Removal mechanism of heavy metal (Cu, Ni, Zn, and Cr) in the presence of cyanide during electrocoagulation using Fe and Al electrodes. Journal of Water Process Engineering, 33, 101109.*

Liu, T., He, F., An, C., Kang, X., Huang, Z., Li, W., & Zhang, Y. (2018). *Experimental study on the treatment of chromium containing wastewater by electric flocculation. IOP Conference Series: Earth and Environmental Science, 170(5).*

Mahmad, M. K. N., Rozainy, M. A. Z. M. R., Abustan, I., & Baharun, N. (2016). *Electrocoagulation Process by Using Aluminium and Stainless Steel Electrodes to Treat Total Chromium, Colour and Turbidity. Procedia Chemistry, 19, 681-686.*

Mamelkina, M. A., Vasilyev, F., Tuunila, R., Sillanpää, M., & Häkkinen, A. (2019). *Investigation of the parameters affecting the treatment of mining waters by electrocoagulation Journal of Water Process Engineering, 32, 100929.*

Martín-Domínguez, A., Rivera-Huerta, M. L., Pérez-Castrejón, S., Garrido-Hoyos, S. E., Villegas-Mendoza, I. E., Gelover-Santiago, S. L., Drogui, P., & Buelna, G. (2018). *Chromium removal from drinking water by redox-assisted coagulation: Chemical versus electrocoagulation Separation and Purification Technology, 200, 266-272.*

Min, K.J., An, H.J., Lee, A.H., Shin, H.-G., Park, K.Y. (2023). *Electrodialysis with a channeled stack for high strength cadmium removal from wastewater, Membr, Water Treat. 14, 47–54.*

Mubarak, A. E., Saleh, O. A., Mohamed, A. M., Isam Y. Q., Mohamed, H., Omer, Y. B., Gaber, A. E., Ahmed, F.F. A., Mohammad, S. A., Mustafa, S. E., Islam, G. A., Zeyad, M. A. (2024). *Enhancing photocatalytic performance of Co-TiO2 and Mo-TiO2-based catalysts through defect engineering and doping: A study on the degradation of organic pollutants under UV light Journal of Photochemistry & Photobiology, A: Chemistry 446, 115164.*

Naghdali, Z., Sahebi, S., Ghanbari, R., Mousazadeh, M., & Jamali, H. A. (2019). *Chromium removal and water recycling from electroplating wastewater through direct osmosis: Modeling and optimization by response surface methodology. Environmental Health Engineering and Management, 6(2), 113-120.*

Nwabanne, J. T., Igwegbe, C. A., & Okpo, S. O. (2018). *Removal of Copper, Nickel, and Chromium from Simulated Wastewater using Electrocoagulation Technique. 2018 International Conference Proceedings: Faculty of Engineering, Unizik, August, 448-458.*

Patil, Y., Attarde, S., Fegade, U., Bakather, O.Y., Ali, S.K. (2023). *Highly efficient removal of a toxic*

methylene blue dye by adsorption on CuAlMnO nanoparticles: adsorption kinetics, isotherm, and mechanism studies using statistical modelling. *International Journal of Environmental Analytical Chemistry*, 1-18.

Pavithra, K. G., Jaikumar, V., Kumar, P. S., & Sundarrajan, P. (2020). Cleaner strategies on the effective elimination of toxic chromium from wastewater using coupled electrochemical/ biological systems *Environmental Progress and Sustainable Energy*, 39(4), e13399.

Peng, H. & Guo, J. (2020). Removal of chromium from wastewater by membrane filtration, chemical precipitation, ion exchange, adsorption electrocoagulation, electrochemical reduction, electrodialysis, electrodeionization, photocatalysis and nanotechnology: a review. *Environmental Chemistry Letters*, 18, 2088-2068.

Peng, H., Leng, Y., & Guo, J. (2019). Electrochemical removal of chromium (VI) from wastewater. *Applied Sciences*, 9(6), 1156.

Petrie, B., Barden, R., & Kasprzyk-Hordern, B. (2015). A review on emerging contaminants in wastewaters and the environment: Current knowledge, understudied areas and recommendations for future monitoring. *Water Research*, 72, 3-27.

Prasetyaningrum, A., Jos, B., Dharmawan, Y., Prabowo, B. T., Fathurrazan, M., & Fyrouzabadi (2018). The influence of electrode type on electrocoagulation process for removal of chromium (VI) metal in plating industrial wastewater. *Journal of Physics: Conference Series*, 1025, 012126.

Sadeghi, S., Alavi Moghaddam, M. R., & Arami, M. (2017). Techno-economical evaluation of hexavalent chromium removal by electrocoagulation process with the aid of polyaluminum chloride as coagulant: Optimization through response surface methodology *Environmental Engineering and Management Journal*, 16(1), 93-104.

Singh, H., Sonal, S., & Mishra, B. K. (2018). Hexavalent chromium removal by monopolar electrodes based electrocoagulation system: Optimization through Box-Behnken design. *Journal of Water Supply: Research and Technology - AQUA*, 67(2), 147-161.

Tejada-Tovar, C., Villabona-Ortíz, A., & Ortega-Toro, R. (2020). Determination of Kinetic Parameters in the Biosorption of Chromium (VI) in Aqueous Solution *Ingeniería y Ciencia*, 16(31), 129-143.

Thirugnanasambandham, K. & Shine, K. (2018). Investigation on the Removal of Chromium from Wastewater using Electrocoagulation *International Journal of Chemical Reactor Engineering*, 16(5), 1-10.

Yan, B., Peng, J., Deng, F., Liu, L., Li, X., Shao, P., Zou, J., Zhang, S., Wang, J., Luo, X. (2023). Novel ZnFe2O4/Bi2S3 high-low junctions for boosting tetracycline degradation and Cr(VI) reduction, *Chem. Eng. J.* 452, 139353.

Ziati, M., Khemmari, F., Aitbara, A., & Hazourli, S. (2018). Reduction of Turbidity and Chromium Content of Tannery Wastewater by Electrocoagulation Process *Water Environment Research*, 90(7), 598-603.

DFT studies of the geometry, electronic structure and vibrational spectra of some 1,3-Benzothiazole derivatives

Ali A. El-Rayyes

Chemistry Department, Faculty of Science, Northern Border University, Arar 1321, Saudi Arabia.

Abstract: Calculated geometrical parameters for some 1,3-benzothiazole derivatives (1,3-BT), namely; 2-vinyl-1,3-benzothiazole, 2-(2-pyridyl)-1,3-benzothiazole, 1,3-benzothiazole-2-carboxaldehyde and 1,3-benzothiazole- 2-carbonyl fluoride were calculated using density functional theory (DFT) at the 6-311++G(d,p) level. Excited state calculations were carried out using the Time Dependent-DFT/6-311++G(d,p) method. 1,3-BT is found to exist in two main conforms, the A form and the B form with the B form to be more stable than the A form with A form to B form rotational barrier ranging from 5.73 Kcal/mol to 9.78 Kcal/mol. HOMO-LUMO energies and the global quantum chemical parameters were determined. For substituted 1,3-BT molecules, the energy difference between HOMO and LUMO was determined to be between 4.70 and 3.95 eV. Both vinyl and formyl substituted BT have the highest and lowest values of η that is 2.35 and 1.98 eV, respectively. Simulated UV and IR spectra were determined with complete assignments of the vibrational frequencies.

Keywords: DFT calculations; Rotational barrier; Vibrational frequencies and spectra, 1,3-benzothiazole derivatives, 2-(2-Pyridyl)-1,3-benzothiazole.

(*) **Corresponding Author**:

Ali A. El-Rayyes, Chemistry Department, Faculty of Science, Northern Border University, Saudi Arabia.

Arar: 1321

E-mail: ali.elrayyes@nbu.edu.sa

دراسة الشكل و التركيب الالكتروني واطياف الاهتزاز لبعض مشتقات مركب 1و3-بنزوثيازول بواسطة نظرية الكثافة الوظيفية

د. علي الريس

جامعة الحدود الشمالية، كلية العلوم، قسم الكيمياء — عرعر — المملكة العربية السعودية

مستخلص البحث: تم التعرف على الاشكال الفراغية لبعض مشتقات -1,3 بنزوثيازول (1,3-BT) وهي؛ -2فينيل-3،1-بنزوثيازول، 2-(2-بيريديل)-3،1-بنزوثيازول، 1،3-بنزوثيازول-2-كربوكسالدهيد و3،1-بنزوثيازول-2-كربونيل فلوريد باستخدام نظرية الكثافة الوظيفية (DFT) عند المستوى 6-311++G(d,p). تم إجراء حسابات الحالة المثارة باستخدام طريقة Time Dependent-DFT/6-311++G(d,p). تم العثور على 3-BT،1 في اثنين من المتناظرات الفراغية، A form & B form ليكون B-form أكثر استقرارًا من الشكل A form مع حاجز الدوران الذي يتراوح من 5.73 كيلو كالوري / مول إلى 9.78 كيلو كالوري / مول. تم تحديد أطياف الأشعة فوق البنفسجية وطاقات HOMO-LUMO و التي تراوحت بين 4.70 و3.95 الكترون فولت وبعض الثوابت الكيميائية الكمومية العالمية، على سبيل المثال الثابت η له قيم تتراوح بين 2.35 و1.98 لكل من مشتق الفينيل و الفورميل. تم تحديد أطياف الأشعة تحت الحمراء المحاكاة مع تعيينات كاملة للترددات الاهتزازية.

كلمات مفتاحية: حسابات نظرية الكثافة الوظيفية، حاجز الدوران، ترددات واطياف الاهتزاز، مشتقات مركب 1و3-بنزوثيازول، 2(2-بيريدايل) 1و3-بنزوثيازول

(*) للمراسلة:

د.علي الريس، جامعة الحدود الشمالية، كلية العلوم، قسم الكيمياء، عرعر، المملكة العربية السعودية.

عرعر: 1321

E-mail: ali.elrayyes@nbu.edu.sa

1. Introduction

Heterocyclic compounds such as benzothiazoles (BT) constituents two fused rings of thiazole and benzene (Téllez,López-Sandoval,Silvia,Castillo-Blum,Barba-Behrens, 2008). Organic and medicinal chemists have been fascinated by benzothiazole and its derivatives as potential pharmaceuticals. Benzothiazole possesses a wide range of biological actions, including anti-inflammatory, anti-tumor, anti-HIV, anti-virus, schistosomicidal, anti-bacterial, and anti-tumor properties.

The benzothiazole molecule has two distinct chromophores: aromatic rings and thiazole. These chromophores have intriguing chemical and biological features that encourage further study of the compounds. Numerous studies on substituted benzothiazoles have revealed a range of biological activity and chemical reactivity. Pharmacological activity such as antiviral (Mubarik, Mahmood, Rasool, Hashmi, Ammar, Mutahir, Ali, Bilal, Akhtar, Ashraf, (2022), antibacterial (Sathyanara, Karunathan, Kannappan, 2013), antimicrobial (Hafizi, Zainal, Mark-lee, Tahir, Ahmad, Kassim, 2018), and fungicidal (Mabrouk, Azazi, Alimi, 2010), are reported for the benzothiazole ring. As anti-allergic (Zahradník,1990), antidiabetic (Bédé, Koné, Kon, Ouattara, Ouattara, Bamba, 2019), anticancer (Tahlan, Kumar, Narasimhan 2019), anti-inflammatory (Chen, Femia, Babich, Zubieta, 2001), anthelmintic (Tariq, Kamboj, Amir 2019), and anti-HIV agents, they are also beneficial. Moreover, condensed pyrimido-benzothiazoles and benzothiazolo-quinazolines exhibit antiviral action, while phenyl substituted benzothiazoles have anticancer activity (Khokr, Arora, Kha, Kaushik, Saini, Husain, 2019; Mishra, Ghanavatkara, Malib, Qureshi, Chaudhari, Sekar, 2019; Yagodzinska, Yagodzinski, Yablonski, 1980).

Computational chemistry has emerged as a fascinating field in recent years for using a laptop or other modern computer to analyze chemical problems (Singhal, Mishra, Datta, 2016; Maji, Sengupta, Chattopadhyay, Mostafa, Schwalbe & Ghosh, 2001; Coni, Massacesi, Ponticelli, Puggioni & Putzolu, 1987; Malik, Manvi, Nanjwade, Singh, Purohit, 2010; Gomathi, Vijayan, Viswanathamurthi, Suresh, Nandhakumar & Hashimoto, 2017; Melnik, Mikuš & Holloway, 2013; Kuramshina, Vakula, Vakula, Majouga, Senyavin, Gorb, Leszczynski, 2016). It is a rapidly developing and informative field that works with the mathematical calculation and visualization of systems, including pharmaceuticals, polymers, biomolecules, and organic and inorganic complexes and molecules.

Due to their distinctive electro-optical properties, these heterocyclic compounds containing electron-rich nitrogen and sulfur heteroatoms have received a lot of attention in recent years (Mishra, Ghanavatkara, Malib,

Qureshi, Chaudhari, Sekar, 2019). In addition to their biological and pharmacological features (Malik1, Manvi, Nanjwade, Singh, Purohit, 2010; Tong, Fu, Ma,2018; Niknam, Hamidizadeh, Nabavizadeh, Niroomand, Hoseini, Ford, Abu-Omar, 2019; He, Vogels, Decken , Westcott, 2004), benzothiazole derivatives may produce a spectrum of colors with good transport properties, which makes them suitable for application in light-emitting diodes (LEDs) as both emissive and electron-transporting materials (Maji, Sengupta, Chattopadhyay, Mostafa, Schwalbe & Ghosh, 2001).

Due to the lack of experimental determination of structure and geometries of some 2-substituted 1,3-benzothiazole (1,3-BT), The present study is to theoretically investigate the geometrical structures, conformations and spectroscopic properties of 2-vinyl-1,3-benzothiazole (VBT), 2-(2-pyridyl)-1,3-benzothiazole (PBT), 1,3-benzothiazole-2-carboxaldehyde (BTC) and 1,3-benzothiazole-2-carbonyl fluoride (BTCF). Density functional theory (DFT) have been used to perform the gas phase calculations for the molecules under study at both ground and excited states. Results of the study could enable researchers to closely look at these molecules as a potential precursor in the preparation of new electro-optical materials.

2. COMPUTATIONAL METHOD

All of the computations have been performed using the density functional theory (DFT) technique, which is included in the Gaussian 09 program package (Frisch et al, 2003). Previous research has demonstrated that the molecular geometry, vibrational frequency, and electrical characteristics of organic molecules have been accurately and consistently determined using DFT methods (Dennington, Keith, & Semichem, 2016; Jamroz, 2004; El-Rayyes, Umar, 2005; El-Rayyes, Maung, 2005; El-Rayyes, Maung, 2004). The calculations in this study were performed utilizing the 6-311G++(d,p) basis set by applying the B3LYP method (El-Rayyes, 2003; El-Rayyes, 2003). GaussView (Dennington, Keith, & Semichem, 2016) was used to create the initial geometries of the molecules under study. After that, unrestricted geometry optimization and frequency calculations were performed. Figure 1 shows the atom numbering in 1,3-BT molecules.

Further calculations, such as electronic parameter, vibrational infrared spectra, and UV-visible spectra of the molecules, were subsequently performed using the newly optimized structural parameters. The electronic absorption spectra were performed using time-dependent density functional theory (TD-DFT) . Using the polarizable continuum model (PCM) and its integral equation formalism variant (IEF-PCM), the UV-visible spectral calculations were performed in methanol (Umar and El-Rayyes, 2024). Based on the potential energy

distribution as previously mentioned (El-Rayyes, Umar, 2005; El-Rayyes, Maung, 2005; El-Rayyes, Maung, 2004; El-Rayyes, 2003; El-Rayyes, 2003; Umar and El-Rayyes, 2024)], normal vibrational modes were identified using the VEDA4 program (Jamroz, 2004). For Gaussian software calculations a z-matrix describing the molecular geometries is used as a data input file, however, for VEDA 4 program the optimized frequescies obtained from DFT calculations is used as input data file.

2.1 Asymmetric torsional potential function

By allowing N=C–CC (N=C–CO in formyl and N=C–CN in the pyridyl derivative) torsional angle (φ) to vary by 15° increments from 0° (A form, where the vinyl double bond (or the carbonyl group) eclipses the N=C bond) to 180° (B form, where the vinyl double bond (or the carbonyl group) is anti to the N=C bond), the potential surface scan for the internal rotation about the C–C single bond was obtained. After identifying the saddle areas, geometry optimization was performed at

the transition states. Furthermore, geometry optimization was performed at each of the fixed torsional angles (φ) [N=C–CC (N=C–CO or N=C–CN)] at 15, 30, 45, 75, 90, 105, 135, 150, and 165. The torsional potential was represented as a Fourier cosine series in the dihedral angle (φ):

$$V(\phi) = V_0 + \sum_n \left(\frac{V_n}{2}\right)[1 - COS(n\phi)]$$

; where the potential coefficients from V1 to V6 are thought to be sufficient to explain the potential function, and V0 is the relative energy of the A form. Using the recursive least squares method, the six coefficients were determined based on the energy optimization results that correspond to (φ) of 0°–180°. Table 1 contains a list of the data. Figure 2 displays the asymmetric potential functions for the internal rotation of the four molecules.
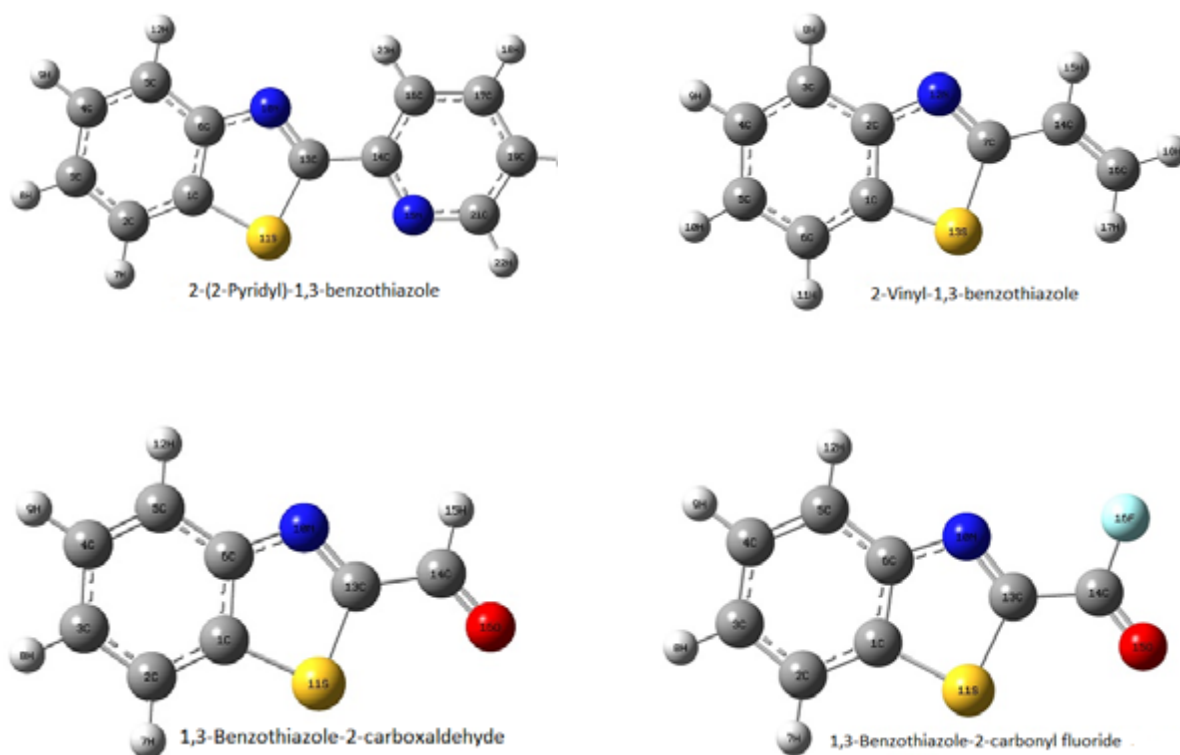

Figure 1: Atom numbering for optimized structures of 1,3-benzothiazole derivatives

3. RESULT

3.1 Molecular geometries:

The DFT-B3LYP optimized geometry parameters for the most stable geometrical structure of the molecules are given in Table 2. The C-C bond lengths were calculated to be in the range of 1.457–1.480 Å, depending on the substituent with the least value found in VBT (1.457 Å) and the highest value in PBT (1.480 Å) indicating more π-bond character in case of VBT. The C=N bond length of thiazole ring varies from 1.294 Å in COF substituent 1.341 Å in 2-pyridyl substituent. This is mainly attributed to the charge effect. The slightly longer values in 2-pyridyl derivative indicated more single bond character due to resonating structures.

When hetero aromatic ring bond distances are compared, it becomes clear that due to differences in electronegativities between substituents and associated atoms the bond distances in hetero aromatic rings are diverging dramatically from one another. The S–C7 bond length is longer than S-C1 bond distance, with higher values found in the longest pyridyl derivative (1.793 Å) and shortest value found with COF substituted BT is 1.768 Å indicating pure single bond. While S-C1 bond length varies from 1.750 Å to 1.745 Å, an average distance for a carbon–sulfur bond and the 1.81 Å which indicate that the actual bond order is between one and two which is due to conjugative effect in benzothiazole. For N=C and N-C2 bond lengths, due to ring strain the N=C double bond distance is 1.297 Å, 1.291 Å, 1.298 Å and 1.294 Å in VBT, PBT, BTC and BTCF respectively.

Symmetry of the thiazole ring is distorted due to substitution effect, yielding ring angles smaller than 120° at the point of substitution. This fact was clear from the calculated S-C-N bond angle in VBT, BTC and BTCF, while it was exactly found to equal 120° in PBT, this suggests a planar configuration due to conjugation between thiazole ring and pyridyl substituent.

Compared to the benzene ring, the heteroring exhibits greater distortion in bond properties. The central atom's electronegativity, the existence of a lone pair of electrons, and the conjugation of the double bonds all affect how much the bond angle varies. The bond angle decreases with decreasing core atom electronegativity. Thus, the bond angle C–S–C is very less (88.6°, 88.6°, 87.9° and 87.9°) in VBT, PBT, BTC and BTCF respectively, than the bond angle C–N–C (111.9°, 112.0°, 111.0°, 110.8°) in VBT, PBT, BTC and BTCF respectively, which is due to the fact that electronegativity of nitrogen is greater than sulfur.

3.2 Energetics

The B3LYP total energies of the four molecules, VBT, PBT, BTC and BTCF in their stable conformations is summarized in Table 3. Free rotation of the C-C bond lead to an equilibrium between the A form and B form with the B form to be the most stable conformation The corrected barrier to interconversion, A form-B form barrier was found to be about 5.005 kcal/mol, 7.435 kcal/mol, 5.058 kcal/mol and 5.390 kcal/mol in VBT, PBT, BTC and BTCF respectively. The high rotational barrier is a result of the possible conjugation where the C-C single bond could have some π-character. This could be explained in terms of electronic effects, where the electron donating vinyl group lead to more delocalized double bond.
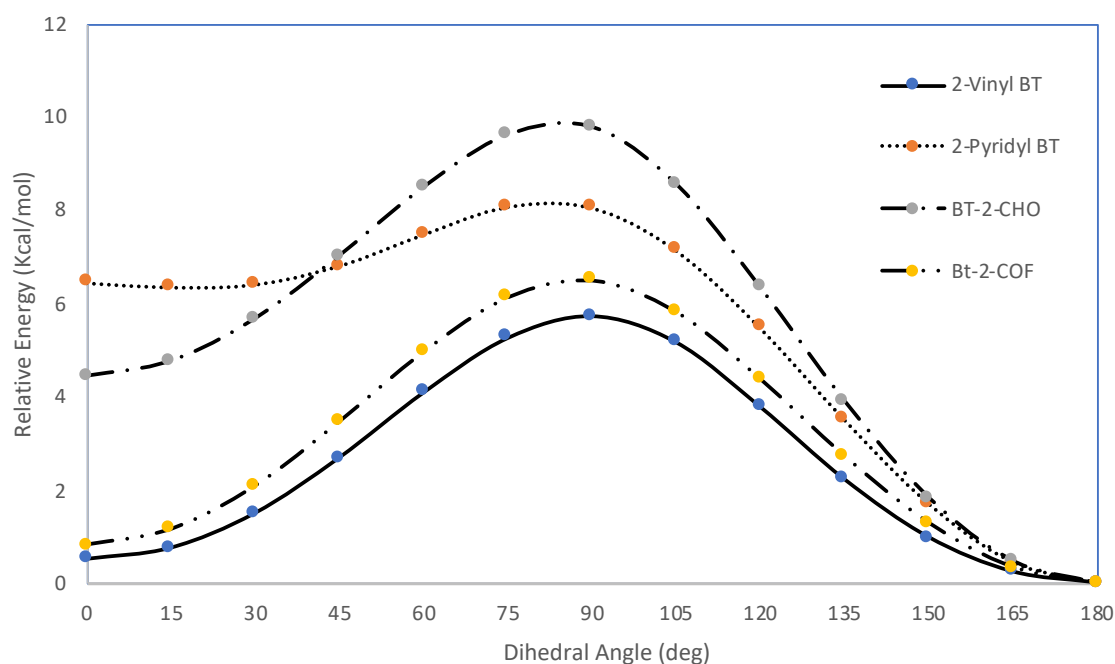

Figure 2: The determined potential surface for 2-vinyl-1,3-benzothiazole (solid line), 2-(2-pyridyl)-1,3-benzothiazole (dotted line), 1,3-benzothiazole-2-carboxaldehyde (dashed line) and 1,3-benzothiazole-2-carbonyl fluoride(dashed-dotted line)

Table 1. Calculated potential coefficients (kcal/mol) for internal rotation in substituted 1,3-BT derivatives calculated at DFT-B3LYP/6-311++G(d,p) level

Parameter	2-Vinyl-1,3-benzothiazole	2-(2-Pyridyl)-1,3-benzothiazole	1,3-Benzothiazole-2-carboxaldehyde	1,3-Benzothiazole-2-carbonyl fluoride
V_1	-0.787	-0.897	-4.352	-0.416
V_2	4.946	5.747	3.100	1.822
V_3	-0.450	-0.520	0.193	0.034
V_4	-0.293	-0.329	-0.293	-0.137
V_5	0.129	0.138	0.129	0.019
V_6	0.021	0.019	0.021	0.038

Table 2. Optimized parameters for substituted1,3-BT derivatives calculated at B3LYP /6-311++G(d,p) level of theory

Parameter[a]	2-Vinyl-1,3-benzothiazole	2-(2-Pyridyl)-1,3-benzothiazole	1,3-Benzothiazole-2-carboxaldehyde	1,3-Benzothiazole-2-carbonyl fluoride
Bond distance (A°)				
R(C=C)	1.336	1.402		
R(C-C)	1.457	1.480	1.477	1.476
R(C=N)	1.297	1.341	1.298	1.294
R(C7-S13)	1.787	1.793	1.768	1.768
R(N-C2)	1.380	1.291	1.376	1.375
R(S13-C1)	1.750	1.747	1.747	1.745
R(C1-C2)	1.414	1.451	1.418	1.418
R(C=O)			1.209	1.188
R(C-F)				1.348
Valence angles (deg)				
∠(SC7N12)	115.0	120.3	116.4	116.6
∠(CSC)	88.6	88.6	87.9	87.9
∠(C7NC2)	111.9	112.0	111.0	110.8
∠(C=C-C7)	126.3	122.2		
∠(C-C-S)	122.3	120.3	121.1	118.3
∠(C-C-N)	122.7	124.9	122.5	125.0
∠(O=C=C)			123.9	126.3
∠(OCH)			122.8	121.6
Dihedral Angles (deg)				
∠(CCCN)	180.0	180.0		
∠(CCCS)	0.0	0.0		
∠(OCCN)			180.0	180.0
∠(OCCS)			0.0	0.0
Rotational Constant (MHz)				
A	2843.8	1877.7	2868.0	2284.8
B	659.3	297.2	655.4	529.1
C	535.2	256.6	533.5	429.6
Dipole Moment (Debye)				
μ	1.09	1.40	3.83	5.25

[a] Atom numbering are provided in Figure 1

Table 3: Computed total energies and/or zero-point corrections (hartrees), and relative energy and rotational barriers (kcal/mol) in 2-substituted benzothiazole calculated at DFT-B3LYP/6-311++G)d,p) level

	2-Vinyl-1,3-benzothiazole	2-(2-Pyridyl)-1,3-benzothiazole	1,3-Benzothiazole-2-carboxaldehyde	1,3-Benzothiazole-2-carbonyl fluoride
Total energy				
cis	-800.2322566	-969.9601537	-836.1577691	-935.4510216
trans	-800.2330631	-969.9703854	-836.1648137	-935.451216
TS	-800.2239564	-969.9575511	-836.1492803	-935.4419881
Relative energy	0.508	6.446	4.438	0.818
cis–trans Barrier	5.229	1.640	5.348	5.691
trans–cis Barrier	5.737	8.086	9.786	6.509
Zero-point correction				
cis	0. 092902	0.064529	0.049464	0.112754
trans	0.092925	0.064508	0.049553	0.112759
TS	0.093258	0.064018	0.049925	0.113230
Corrected relative energy	0.494	6.359	4.382	0.815
Corrected cis–trans barrier	5.005	1.318	5.058	5.390

3.3 Electronic Properties and Energy Profile

The highest occupied molecular orbitals (HOMO) and the lowest unoccupied molecular orbitals (LUMO) three-dimensional graphs for the four benzothiazole compounds obtained via optimization and frequency calculations are shown in Figure 3. The electronic characteristics of the four benzothiazole compounds, including oscillator strengths and excitation energies, were calculated using the TD-DFT/IEFPCM method. The HOMO and LUMO patterns and their energies are displayed in Figure 3. The absorption spectra of the four benzothiazole compounds are displayed in Figure 4. Every molecule has a unique absorption peak in the methanol medium. The electron transfer from the ground state to the excited state is correlated with the associated excitation energy of each absorption peak.

The most likely absorption wavelengths for benzothiazoles are listed in Table 4, along with the principal molecular orbital contributions, oscillator strengths, and molecular orbital assignments that correspond to them in the methanol medium. The electron transfer from the ground state to the excited state is correlated with the associated excitation energy of each absorption peak. The most likely absorption wavelengths for benzothiazoles are listed in Table 4, along with the principal molecular orbital contributions, oscillator strengths, and molecular orbital assignments that correspond to them.

The electronic excitation wavelengths of the envisioned spectra were found to be between 228 and 370 nm, as shown in Figure 4. It is clear that the different absorption wavelengths of the BT compounds are caused by the unique electronic characteristics of the substituent. The HOMO and LUMO energy values are used to determine the global reactivity descriptors, which include ionization potentials (IP), hardness (η), chemical potential (μ), chemical softness (S), and the electrophilicity index (ω). The global reactivity descriptors and the calculated HOMO, LUMO, and HOMO-LUMO energy values are shown in Table 5.

The lowest energy electronic excitation permitted in the molecules under study, recognized as the HOMO-LUMO energy gap, which is the difference between the HOMO and LUMO energies. The electrons ability to move determines how energy is distributed properly across the molecule in large conjugated systems, stabilizing it. Therefore, a lower HOMO-LUMO energy gap suggests a more chemically stable system. The energy difference between HOMO and LUMO for BT molecules was found to be between 4.70 and 3.95 eV. With an energy gap of 4.70 eV, the vinyl derivative is considered to have more chemically stable structure than the formyl derivative, which has the least stable structure with HOMO-LUMO energy gab of 3.95 eV, as seen in Table 5.

Table 4: Calculated absorption wavelength (λ), excitation energies (E), and oscillator strengths (f) for substituted1,3-BT derivatives at TD-DFT/B3LYP/6–311++ G(d,p)

	l(nm)	E(eV)	f	cont	Assignments*
2-Vinyl-1,3-benzothiazole	303	4.09	0.0645	68	42 -> 43
	282	4.40	0.5112	66	41 -> 43
	261	4.74	0.0001	99	40 -> 43
	240	5.16	0.0003	76	42 ->45
	234	5.30	0.0391	46	42 -> 44
	229	5.41	0.0005	78	41 -> 45
2-(2-Pyridyl)-1,3-benzothiazole	l(nm)	E(eV)	f	cont	Assignments*
	316	3.92	0.5937	86	55 -> 56
	309	4.01	0.0835	79	54 -> 56
	299	4.14	0.0305	89	53 -> 56
	270	4.58	0.0124	66	52 -> 56
	268	4.62	0.0209	72	55 -> 57
	266	4.65	0.0038	82	53 -> 57
1,3-Benzothiazole-2-carboxaldehyde	l(nm)	E(eV)	f	cont	Assignments*
	370	3.35	0.0271	79	42 -> 43
	361	3.44	0.0096	67	40 -> 43
	324	3.82	0.3810	85	41 -> 43
	301	4.11	0.0362	84	39 -> 43
	246	5.05	0.0074	89	38 -> 43
	229	5.41	0.0268	43	42 -> 45
1,3-Benzothiazole-2-carbonyl fluoride	l(nm)	E(eV)	f	cont	Assignments*
	367	3.38	0.0342	96	46 -> 47
	323	3.84	0.3446	86	45 -> 47
	304	4.07	0.0801	87	44 -> 47
	272	4.57	0.0001	94	42 -> 47
	244	5.08	0.0125	89	43 -> 47
	228	5.43	0.0474	51	46 -> 50
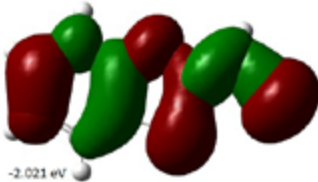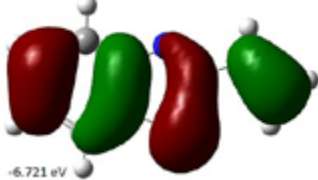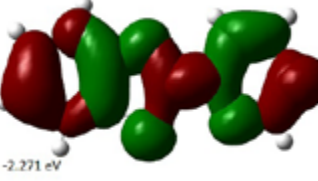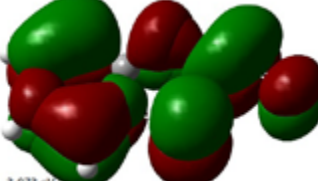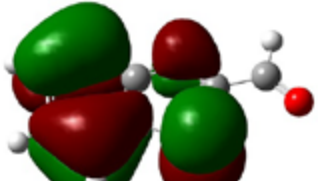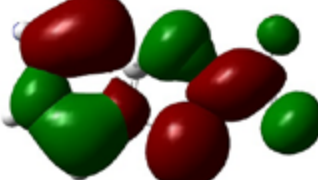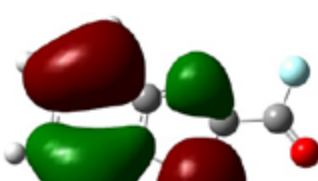
2-Vinyl-1,3-benzothiazole	**LUMO**	
	HOMO	
2-(2-pyridyl)-1,3-benzothiazole	**LUMO**	
	HOMO	
1,3-benzothiazole-2-carboxaldehyde	**LUMO**	
	HOMO	
1,3-benzothiazole- 2-carbonyl fluoride	**LUMO**	
	HOMO	

Figure 3. HOMO and LUMO patterns for substituted1,3-BT derivatives calculated by B3LYP/6–311++G(d,p).

34

The HOMO and LUMO energies can be used to calculate many quantum chemical properties, such as electronegativity (χ), chemical hardness (η), softness (s), potential (μ), and electrophilicity (ω). Since it evaluates the resistance to charge transfer, the η, which represents the molecule's propensity for charge transfer, is an effective means for validating chemical processes [Umar and El-Rayyes, 2024]. The highest and lowest values of η for substituted BT are 2.35 and 1.98 eV, for vinyl and formyl substituted BT respectively. Given this, it is easy to determine that the softest molecule that is most prone to chemical reactions and charge transfer is formyl BT.

A molecule with a higher χ value is an electron acceptor that is superior to other molecules. The vinyl and COF derivatives have the lowest and highest values' χ values have been determined to be 4.37 and 5.16 eV, respectively. The high χ values linked to COF derivatives may be primarily caused by the presence of fluoride atoms. The alkenyl and aryl groups' ability to donate electrons is the primary cause of the fall in χ parameter values observed in both vinyl and pyridyl derivatives.

The electrophilicity index (ω) classifies systems according to their capacity of taking away electrons from their environment in order to take up additional electronic charge. The BT molecules substituted with CHO and COF have the largest ω parameter, measuring 6.45 and 6.72 eV, respectively.
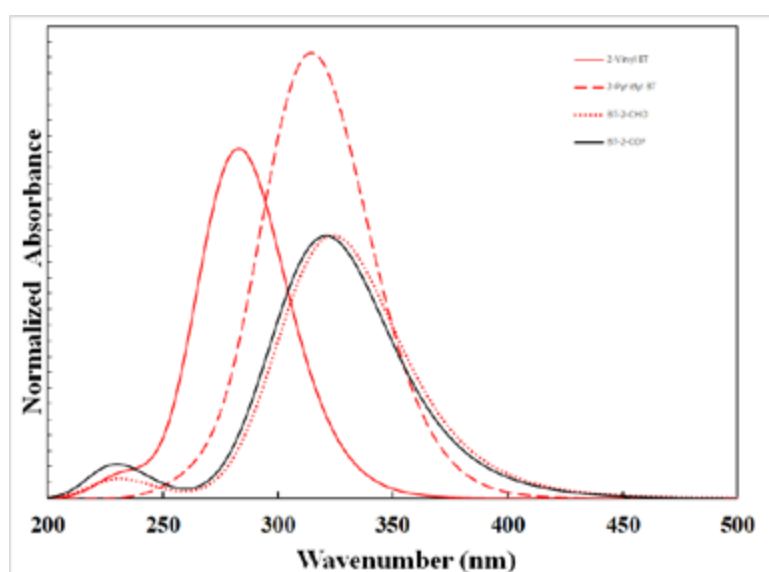
Figure 4: UV spectra of substituted 1,3-benzothiazole molecules.

Table 5 Calculated HOMO and LUMO energies, HOMO-LUMO energy gap, and global reactivity descriptors for substituted 1,3-BT

Propertya	2-Vinyl-1,3-benzothiazole	2-(2-Pyridyl)-1,3-benzothiazole	1,3-Benzothiazole-2-carboxaldehyde	1,3-Benzothiazole-2-carbonyl fluoride
EHOMO (eV)	-6.7210	-6.6571	-7.0274	-7.1346
ELUMO (eV)	-2.0207	-2.2705	-3.0726	-3.1796
$|\Delta E|$ = EHOMO - ELUMO gap (eV)	4.70	4.39	3.95	3.96
Ionization potentials (I)	6.72	6.66	7.03	7.13
Electron affinity (A)	2.02	2.27	3.07	3.18
Electronegativity (χ)	4.37	4.46	5.05	5.16
Chemical hardness (η)	2.35	2.19	1.98	1.98
Chemical potential (μ)	-4.37	-4.46	-5.05	-5.16
Chemical softness (S),	0.21	0.23	0.25	0.25
Electrophilicity index (ω)	4.06	4.54	6.45	6.72

[a] $I = - E_{HOMO}$ (eV), $A = - E_{LUMO}$ (eV), $\chi = (I + A)/2$ (eV), $\eta = (I - A)/2$ (eV), $\mu = -(I + A)/2$ (eV), $S = 1/(2\eta)$ (eV^{-1}), $\omega = \mu^2/2\eta$ (eV)

3.4 Vibrational IR spectral properties

For the more stable conformer, the B form conformer, figure 5 shows the calculated vibrational spectra for the molecules and tables 6 and 7 include the determined vibrational wavenumbers and their associated intensities as well as the proposed vibrational mode assignments.

3.4.1   C–H Stretching

Owing to aromatic C–H stretching vibrations, Aromatic compounds are known to exhibit numerous weak bands in the 3100–3000 cm−1 area (Tariq, Kamboj, Amir 2019; Khokr, Arora, Kha, Kaushik, Saini, Husain, 2019; Mishra, Ghanavatkara, Malib, Qureshi, Chaudhari, Sekar, 2019; Yagodzinska, Yagodzinski, Yablonski, 1980). The C–H stretching vibrations in the current case are recorded between 3200 and 3140 cm−1. In benzothiazoles, an experimental Ar-CH stretching vibration of 3056 cm-1 has been reported (Mishra, Ghanavatkara, Malib, Qureshi, Chaudhari, Sekar, 2019). The region between 1300 and 1000 cm−1 is where the aromatic C–H in-plane bending modes of benzene and its derivatives are detected. The medium intensity C–H out-of-plane bending modes (Tariq, Kamboj, Amir 2019; Khokr, Arora, Kha, Kaushik, Saini, Husain, 2019; Mishra, Ghanavatkara, Malib, Qureshi, Chaudhari, Sekar, 2019; Yagodzinska, Yagodzinski, Yablonski, 1980; Singhal, Mishra, Datta, 2016), often capture in the 950–600 cm−1 range. When it comes to BT, the bands that are seen between 1200 and 960 cm−1 are attributed to the C–H in-plane bending vibrations. Within the range of 1000–600 cm−1, the C–H out of plane bending mode of benzene derivatives is detected. The medium to weak bands found at 1014 and 978 cm−1   in the infrared spectrum is assigned to the aromatic C–H out of plane bending vibrations of BT. There is a significant overlap between the in-plane and out-of-plane ring C–C–C bending modes and the aromatic C–H bending vibrations.

3.4.2   C–S Stretching

Because of their high polarizability, the C–S bonds exhibit greater spectral activity. The predicted range for the C–S stretching vibration is 710–685 cm−1 (Khokr, Arora, Kha, Kaushik, Saini, Husain, 2019). Benzothiazoles were found to exhibit C-S stretching vibrations with an experimental value of 706 -672 cm−1 (Yagodzinska, Yagodzinski, Yablonski, 1980). For the molecules under investigation, the C–S stretching vibrations have been identified in the 682–714 cm−1 area. The computed frequencies of 714, 682, 698, and 714 cm−1 are in perfect agreement with both the data from the literature and experimental observation. The C-S vibration is clearly a pure mode, as Tables 6 and 7 demonstrate. Additionally, there is an equivalent correlation between the in-plane and out-of-plane C-S stretching vibration and experimental observations.

3.4.3   C=N Vibrations

The region 1672–1566 cm−1 is where the C=N stretching vibrations (Khokr, Arora, Kha, Kaushik, Saini, Husain, 2019; Mishra, Ghanavatkara, Malib, Qureshi, Chaudhari, Sekar, 2019) has been observed. For BT molecules, the corresponding bands in the IR spectra at 1634, 1488, 1541, and 1555 592 cm−1 are attributed to the C=N stretching vibration. Tables 6 and 7 display the bands that correspond to the C–C–C and C–S–C in-plane and out-of-plane bending modes of BT. According to normal coordinate analysis, there is a noticeable blending of C-H and C-C-C in-plane bending. Similarly, there is a large overlap between the C–H out of plane bending modes and the skeleton out of plane bending modes.

3.4.4   Ring Vibrations

The benzene ring's carbon–carbon stretching modes are predicted to lie between 1650 and 1200 cm−1, and they are typically not highly sensitive to minor substituent substitution; however, the frequency gets reduced by heavy halogens (El-Rayyes, Umar, 2005; El-Rayyes, Maung, 2005; El-Rayyes, Maung, 2004; El-Rayyes, 2003; El-Rayyes, 2003; Umar and El-Rayyes, 2024)]. The computed theoretical values for carbon-carbon stretching modes range from 1653 to 1208 cm−1. These values exhibit good agreement with previously published experimental data of 1654, 1612, and 1485 cm−1 (Khokr, Arora, Kha, Kaushik, Saini, Husain, 2019; Mishra, Ghanavatkara, Malib, Qureshi, Chaudhari, Sekar, 2019; Yagodzinska, Yagodzinski, Yablonski, 1980). The infrared band at 873 cm−1 corresponds to the BT ring's C–C–C in-plane bending vibrations. Together with the C-H in-plane bending vibrations, the C-C in-plane bending vibrations were observed as a combined vibrational mode. In the FTIR spectra for BT, the bands corresponding to C–C–C out-of-plane bending vibrations are seen at 585 and 531 cm−1.

3.4.5   C=O vibrations

In the infrared spectra of 1,3-benzothiazole-2-carboxaldehyde and 1,3-benzothiazole-2-carbonyl fluoride, the C=O stretching frequency is identified as the most intense band. The most stable trans conformers exhibit this line at 1859 cm−1, which was further blue-shifted for the COF group and identified at 1764 cm−1 for the CHO group (mode υ6).
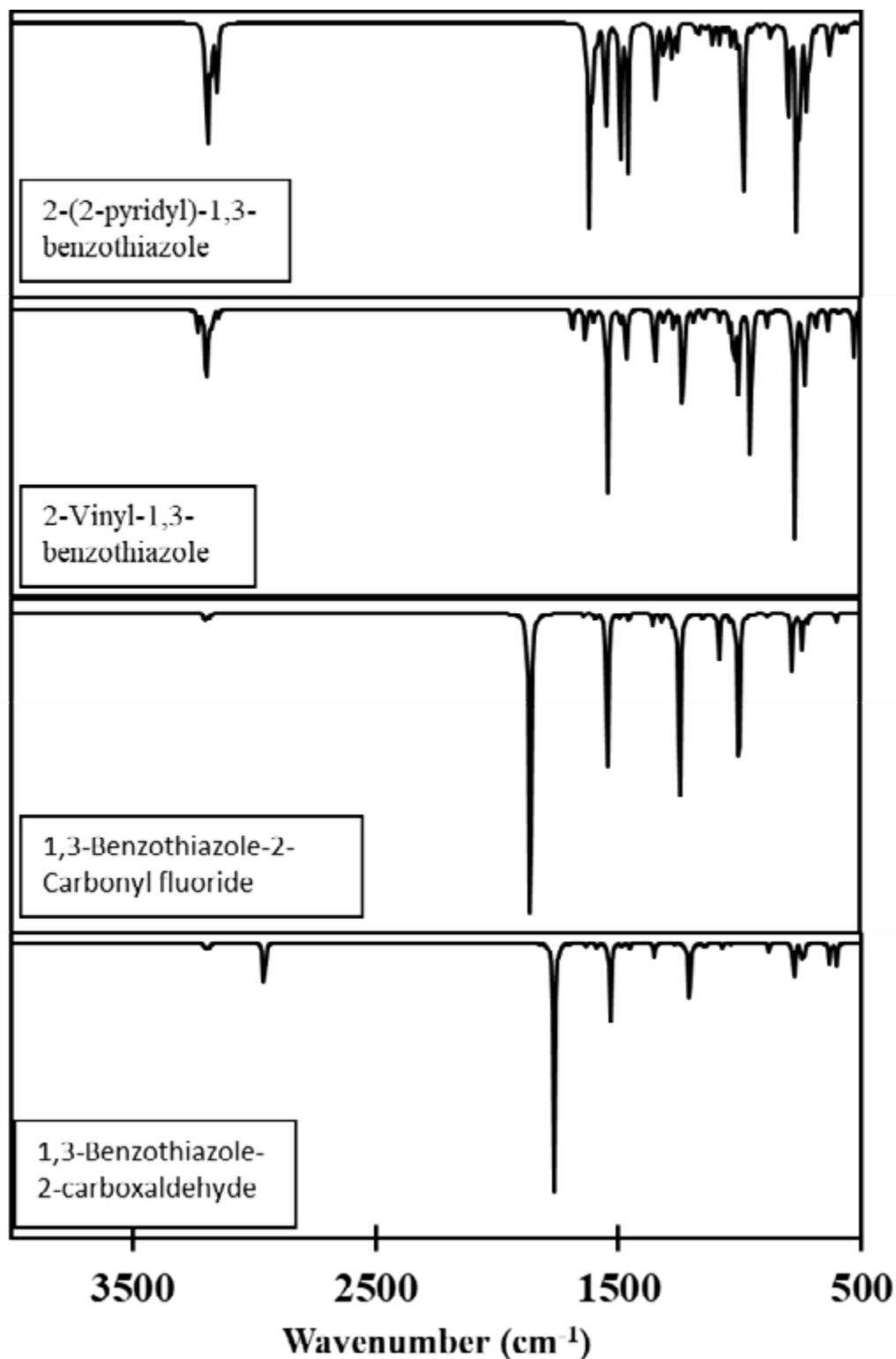
Figure 5: Vibrational IR spectra of substituted 1,3-BT molecules.

Table 6: Calculated vibrational wavenumber (cm⁻¹) for 1,3-Benzothiazole-2-carboxaldehyde and 1,3-Benzothiazole-2-carbonyl fluoride

No	1,3-Benzothiazole-2-carboxaldehyde			1,3-Benzothiazole-2-carbonyl fluoride		
	IR.[a]	Intensity[b]	Assignment[c] (PED ≥ 10%)	IR[a]	Intensity[b]	Assignment[c] (PED ≥ 10%)
ν1	3202	9.15	νCH(97)	3204	6.55	νCH(82)
ν2	3195	10.72	νCH(90)	3197	9.26	νCH(96)
ν3	3185	5.63	νCH(86)	3187	5.38	νCH(97)
ν4	3173	1.60	νCH(96)	3175	1.70	νCH(97)
ν5	2959	94.23	νCH(100)	1859	1024.48	νOC(100)
ν6	1764	860.19	νOC(93)	1635	10.45	νOC(93)
ν7	1634	11.20	νNC(67)	1588	12.94	νCC(63)
ν8	1588	13.32	νCC(63)	1539	423.21	νCC(55)
ν9	1534	316.16	νCC(71)	1488	14.46	νNC(69)
ν10	1488	14.08	νCC(79)	1453	32.49	νCC(34)+ δHCC(43)
ν11	1454	27.44	νCC(57)	1351	35.30	δCCC(14)+ δHCC(49)
ν12	1371	1.28	νCC(67)	1315	27.77	νSC(64)
ν13	1351	60.67	νNC(69)	1269	34.50	νNC(29)+ δHCC(49)
ν14	1309	0.01	νCC(64)	1242	895.00	νCC(14)+νNC(21)+δHCC(34)
ν15	1267	4.27	νSC(83)	1189	1.90	νCC(29)+νFC(17)+δOCF(13)+δCNC(12)
ν16	1208	415.55	νCC(37)+δCCN(39)	1145	24.57	νCC(18)+δHCC(56)
ν17	1187	15.85	δHCC(68)	1079	199.28	νCC24+δHCC(44)
ν18	1145	28.38	νCC(12)+δHCC(52)	1035	23.24	νSC(17)+δCCC(43)+δHCC(10)
ν19	1071	22.19	νSC(20)+δCCC(46)	999	0.05	νCC(59)+δHCC(18)
ν20	1034	7.88	νCC(67)+δHCC(21)	998	1005.22	τHCCC(76)
ν21	1001	0.67	δHCCS(68)+δOCCS(26)	965	5.75	νFC(43)+δCNC(26)
ν22	995	0.13	δHCCC(64)+τCCCC(11)	883	16.01	τHCCC(80)
ν23	963	6.39	δHCCC(79)	867	4.22	νCC(12)+νNC(16)+δCCC(32)
ν24	881	58.37	νNC(13)+δCCC(58)	777	309.97	HCCC(88)
ν25	867	3.23	τHCCC(83)	749	16.10	τHCCC(67)
ν26	777	260.21	τHCCC(69)+τCCCC(20)	736	58.89	τOCFC(78)+τCNSC(10)
ν27	746	100.31	δCCO(64)	735	146.54	δNCC(25)+δCCF(17)
ν28	738	137.41	τHCCC(43)+τCCCC(36)	715	48.01	τHCCC(20)+τCNSC(35)+τCCCC(16)
ν29	714	6.50	νSC(25)+δCCC(46)	698	9.33	νSC(27)+δCCC(43)
ν30	630	196.64	δCCC(28)+δCCN(31)	596	58.98	νFC(11)+δOCF(38)+δCNC(10)+δNCC(10)
ν31	602	236.60	δCCC(40)+ δCCN(18)	595	2.70	δCCC(56)
ν32	601	0.20	τCCCC(63)+τSCCC(13)	512	0.60	δCCC(56)+τSCCC(13)
ν33	510	1.81	νSC(25)+δSCC(21)+δCCC(28)			
ν34	505	5.91	δCCC(15)+τSCCC(58)			

[a] Calculated IR vibrational wavenumbers, cm⁻¹(scaled with 0.9619). [b] Calculated infrared intensities in km mol⁻¹.
[c] ν is stretching, δ is bending, and τ is torsion

Table 7: Calculated vibrational wavenumber (cm^{-1}) for 2-(2-Pyridyl) 1,3-benzothiazole and 2-Vinyl-1,3-benzothiazole.

No	2-(2-Pyridyl)-1,3-benzothiazole			2-Vinyl-1,3-benzothiazole		
	IR.[a]	Intensity[b]	Assignment[c] (PED ≥ 10%)	IR[a]	Intensity[b]	Assignment[c] (PED ≥ 10%) cccccccc
ν1	3211	2.37	νCH(93)	3229	6.69	ν(CH) 95
ν2	3198	15.88	νCH(97)	3200	10.19	ν(CH)93
ν3	3195	20.43	νCH(93)	3193	12.99	ν(CH)93
ν4	3191	19.38	νCH(96)	3182	5.87	ν(CH)92
ν5	3180	6.84	νCH(96)	3170	1.18	ν(CH)92
ν6	3175	10.30	νCH(94)	3169	2.87	ν(CH)96
ν7	3169	1.28	νCH(97)	3142	2.08	ν(CH)97
ν8	3155	27.76	νCH(93)	1683	7.57	ν(CC) 62+δ(HCC)10+δ(HCC)11
ν9	1635	6.55	νCC(61)+δHCC(11)	1630	7.78	ν(CC)51
ν10	1623	127.51	νCC(53)	1594	3.52	ν(CC)59 +δ(HCC) 11
ν11	1607	58.12	νCC(62)+δHCC(10)	1541	45.41	ν(SC)11 + ν(NC)63
ν12	1592	12.15	νCC(50)	1487	4.26	δ(HCC)20 +
ν13	1555	73.71	νNC(69)	1462	12.49	δ(HCC) 51+ ν(CC)14
ν14	1494	125.02	νCC(20)+δHCC(16)+δHCN(31)	1442	0.34	δ(HCC)68 + ν(NC)11
ν15	1486	9.62	νCC(29)+δHCC(46)	1346	14.71	ν(CC)64 + δ(HCC)29+δ(HCC)10
ν16	1464	100.07	δHCC(49)	1310	2.95	δ(HCC)10+δ(HCC) 71
ν17	1460	4.01	δHCC(56)	1302	0.45	δ(HCC)14+δ(HCC)59
ν18	1348	80.77	νCC(51)	1266	4.60	δ(CCN)34+ν(CC)10
ν19	1321	7.18	νNC(26)+δHCN(26)	1229	36.37	δ(CCN)17+δ(HCC)24+ν(CC)35
ν20	1313	26.62	νCC(22)	1184	2.90	δ(HCC)17+δ(HCC)66
ν21	1306	5.41	νNC(59)	1144	3.09	δ(HCC)24+δ(HCC)56
ν22	1279	34.04	νCC(18)+δHCC(27)	1077	2.74	ν(SC)48+δ(CCC)26
ν23	1261	23.83	νNC(28)+δHCC(10)	1038	5.11	ν(CC)19+ν(CC)67
ν24	1185	6.36	νCC(12)+δHCC(66)	1018	16.44	τ(HCCH)94
ν25	1172	14.26	νCC(11)+δHCC(73)	999	23.26	δ(HCC)62
ν26	1144	7.11	νCC(14) + δHCC(41)	986	0.00	τ(HCCC)93
ν27	1114	19.43	νNC(14)+νCC(19)+δHCC(46)	953	0.07	τ(HCCC)87
ν28	1085	18.88	νSC(16)+δCCC(32)	950	45.88	τ(HCCH)97
ν29	1065	6.06	νCC(29)+δCCC(25)	884	4.85	δ(CCC)15+ ν(SC)17+δ(CCC)47
ν30	1036	20.38	νCC(59)+δHCC(26)	862	0.86	τ(HCCS)3
ν31	1016	0.20	τHCCC(73)s	769	56.31	τ(HCCC)94
ν32	1012	29.82	νNC(29)+δCNC(13) +δCCC(41)	730	21.51	τ(CCCC)93
ν33	989	204.46	δCNC(44)	718	4.93	τ(HCCN)96
ν34	985	0.59	τHCCC(69)	716	2.20	ν(CC)53+δ(CCN)18
ν35	984	2.10	τHCCC(73)	682	6.11	ν(SC)14+ν(SC)53+δ(CCN)10
ν36	952	6.52	τHCCC(70)+τCCCC(17)	632	5.92	ν(NC)36+ν(CC)14+δ(HCC) 15
ν37	917	2.94	τHCCC-84	586	1.20	τ(HCCC)91
ν38	874	15.43	νNC(13)+δCCC(23)+δCCC(13)	525	11.65	δ(HCC)22+δ(HCC)52
ν39	860	3.48	τHCCC(84)	509	0.41	ν(CC)45+ν(CC)15+ν(CC)16
ν40	801	175.47	τHCCC(49)+τSCCC(17)τCCCN(20)			
ν41	769	284.52	τHCCC(64)+τCCCC(11)			
ν42	756	125.75	τHCCC(17) + τHCCC(24)+τCNCC(41)			
ν43	730	87.59	τHCCC(32)+τCCCC (40)			
ν44	725	71.84	δCCC(44)+δCCN(12)			
ν45	714	45.67	νSC(30)+δCCC(15)+δCCC(23)			
ν46	691	12.86	δCCC(17)+δCCC(11)+δCCC(16)+δCCN(13)			
ν47	633	47.67	δCCC(73)			
ν48	629	21.71	τSCCC(12)+τCCCC(39)+τCCCN(13)			
ν49	585	26.92	δCCN(11)+δCCC(17)+δCCC(13)+δCCC(19)			
ν50	561	15.78	τCCCC(54)			
ν51	511	0.47	νSC(26)+δCCC(47)			

[a] Calculated IR vibrational wavenumbers, cm^{-1}(scaled with 0.9619). [b] Calculated infrared intensities in km mol^{-1}.

[c] ν is stretching, δ is bending, and τ is torsion

4. Conclusion

The geometrical structure of four substituted 1,3-BT molecules have been optimized using the B3LYP/6-31G(d,p) method without any symmetry constraints. Simulated UV-vis and IR, spectra were used to describe the spectroscopic properties of the molecules. Excited state calculations were carried out using the Time Dependent-DFT/6-311++G(d,p)   method.

1,3-BT is found to exist in two main conforms, the A form and the B form with the B form to be more stable than the A form conformer with A to B form rotational

barrier ranging from 5.73 Kcal/mol to 9.78 Kcal/mol. Symmetry of the thiazole ring is distorted due to substitution effect, yielding ring angles smaller than 120° at the point of substitution.

UV-vis spectra, HOMO-LUMO energies and the global quantum chemical parameters were determined. Simulated IR spectra were determined with complete assignments of the vibrational frequencies. For substituted 1,3-BT molecules, the energy difference between HOMO and LUMO was determined to be between 4.70 and 3.95 eV which demonstrates that vinyl derivative is chemically

more stable structure with an energy gap of 4.70 eV, whereas formyl derivative is the least stable, having an energy gap of 3.95 eV.

Both VBT and BTC have the highest and lowest values of η that is 2.35 and 1.98 eV, respectively. In light of this, it is simple to conclude that formyl BT is the softest molecule and the most susceptible to charge transfer and chemical reactions. In comparison to other molecules, a molecule with a greater χ parameter is a superior electron acceptor. χ values for both VBT and BTCF derivatives were having the lowest and greatest values and were determined to be 4.37 and 5.16 eV, respectively. The presence of fluoride atom can be the main cause for the high χ parameters associated with COF derivatives. Values for χ parameters decrease for both vinyl and pyridyl derivatives due mainly to the electron donating power of the alkenyl and aryl groups.

DATA AVAILABILITY STATEMENT:

The data that support the findings of this study are available on request from the corresponding author.

CONFLICTS OF INTEREST:

The author declares no conflict of interest, financial or otherwise.

ACKNOWLEDGEMENT:

Support from Northern Border University is gratefully acknowledged.

5. REFERENCES

Fabiola T., Horacio L., Silvia E. Castillo-Blum, and Noráh B. (2008). *Coordination behavior of benzimidazole, 2-substituted benzimidazoles and benzothiazoles, towards transition metal ions.* Ark. 245-275. https://doi.org/10.3998/ark.5550190.0009.519

Mubarik A., Mahmood S. Hashmi, M.A. Ammar, Mutahir M., Ali, K., Bilal, M., Akhtar, N., Ashraf, G.A. (2022). *Computational Study of Benzothiazole Derivatives for Conformational, Thermodynamic and Spectroscopic Features and Their Potential to Act as Antibacterials.* Crystals, 12, 912. https://doi.org/10.3390/cryst12070912

Sathyanarayanmoorthi V., Karunathan R., and Kannappan V. (2013). *Molecular Modeling and Spectroscopic Studies of Benzothiazole.* J. of Chem., http://dx.doi.org/10.1155/2013/258519

Muhd Z., Mark L., Syahidah T, Ishak, A., Mohammad K. (2018). *Experimental and DFT Investigation on the Influence of Electron Donor-Acceptor on the Hydrogen Bonding Interactions of 1-(1,3-Benzothiazol-2- y1)-3-(R-benzoylthiourea).* Sains Malay., 47(5): 923–929. http://dx.doi.org/10.17576/jsm-2018-4705-07

Mabrouk A., Azazi A., Alimi K., (2010). *On the properties of new benzothiazole derivatives for organic light emitting diodes (OLEDs): A comprehensive theoretical study.* J. Phys. and Chem Solids 71, 1225-1235.

Zahradník P. (1990). *Quantum-chemical study of electronic structure and transmission of substituent effects in benzothiazole derivatives.* Chem. Papers 44 (2) 145–150.

Lucie A. Bédé, Mawa Koné, Guy R. M. Kon, Simplice C. S. Ouattara, Lamoussa Ouattara, El Hadji S. Bamba (2019). *Tautomeric Equilibrium Modeling: Stability and Reactivity of Benzothiazole and Derivatives.* Intern. J. Chem., 11(1), 84-95.

Sumit Tahlan, Sanjiv Kumar and Balasubramanian Narasimhan (2019). *.Antimicrobial potential of 1H-benzo[d] imidazole scaffold: a review.* BMC Chem.,13-18. https://doi.org/10.1186/s13065-019-0521-y

Xiaoyuan Chen, Frank J. Femia, John W. Babich, Jon Zubieta (2001). *Spectroscopic and structural studies of complexes of the fac-[Re(NSN)(CO)3L]n_ type (NSN_2-(2-pyridyl)benzothiazole; L_Cl, Br, CF3SO3 _, CH3CN).* Inorg. Chim. Acta, 314, 91–96.

Sana Tariq, Payal Kamboj, Mohammad Amir (2019). *Therapeutic advancement of benzothiazole derivatives in the last decennial period.* Arch Pharm Chem Life Sci., 352(1): e1800170. https://doi.org/10.1002/ardp.201800170.

Sukhbir L. Khokr, Kanika Arora, Shah A. Kha, Pawan Kaushik, Reetu Saini and Asif Husain (2019). *Synthesis, Computational Studies and Anticonvulsant Activity of Novel Benzothiazole Coupled Sulfonamide Derivatives.* Iran. J. Pharm. Res. 18 (1), 1-11.

Virendra R. Mishra, Chaitanny W. Ghanavatkara, Suraj N. Malib, Shahnawaz. Qureshi, Hemchandra K. Chaudhari, Nagaiyan Sekar (2019). *Design, synthesis, antimicrobial activity and computational studies of novel azo linked substituted benzimidazole, benzoxazole and benzothiazole derivatives.* Comp. Biol. Chem., 78, 330–337.

Yagodzinska E., Yagodzinski T., and Yablonski Z., (1980). *Synthesis and Spectrometric Investigation of the Thioa.Mides of Thiazole- and Benzothiazole-2-Carboxylic Acids.* Khim. Get. Soed., 9,1287.

Nancy Singhal, Anasuya Mishra, and Anindya Datta (2016). *Excited-State Proton Transfer and Conformational Relaxation of 2-(4'-Pyridyl) benzimidazole in Nafion Films.* Chem. Phys. Chem., 17, 3004 – 3009. https://doi.org/10.1002/cphc.201600546.

Milan Maji, Parbati Sengupta, Shyamal Kumar Chattopadhyay, Golam Mostafa, Schwalbe C. H., Saktiprosad Ghosh (2001). *An unusual ruthenium(ii) complex of 2-(2-pyridyl)*

benzothiazole. *J. Coord. Chem, 54(1), 13-24.* https://doi.org/10.1080/00958970108022626.

Giovanni Coni, Marcella Massacesi, Gustavo Ponticelli, Giovanna Puggioni and Costantino Putzolu (1987). *Palladium (II) and platinum(II) chloride and bromide complexes with some 2-methylpyridyl- or methylquinolyl-benzimidazole, benzoxazole, or benzthiazole. Trans. Met. Chem., 12, 379-381.*

Jitender K Malik, Manvi F. V., Nanjwade B. K., Sanjiv Singh, Pankaj Purohit, (2010). *Review of the 2-Amino Substituted Benzothiazoles: Different Methods of the Synthesis. Der Pharm. Lett., 2 (1) 347-359.*

Asaithambi Gomathi, Paranthaman Vijayan, Periasamy Viswanathamurthi, Shanmugam Suresh, Raju Nandhakumar, Takeshi Hashimoto (2017). *Organoruthenium (II) compounds with pyridyl benzoxazole/ benzthiazole moiety: studies on DNA/ protein binding and enzyme mimetic activities. J. Coord. Chem., 70(10), 1645–1666.* https://doi.org/10.1080/00958972.2017.1309649.

Milan Melnik, Peter Mikuš and Clive Eduard Holloway, (2013). *Platinum organometallic compounds: classification and analysis of crystallographic and structural data of monomeric five and higher coordinated. Rev. Inorg. Chem., 33(1) 13–103.* https://doi.org/10.1515/revic-2013-0001.

Kuramshina G. M., Vakula O. A., Vakula N. I., Majouga A. G., Senyavin V. M., Leonid G. Gorb, Jerzy Leszczynski (2016). *Conformations vibrational spectra and force field of 1-methyl-2-(2-pyridyl)benzimidazole: experimental data and density functional theory investigation in comparison with 2-(2-pyridyl)benzimidazole", Struct. Chem.27, 209–219.* https://doi.org/10.1007/s11224-015-0693-6.

Jitender K Malik, Manvi F. V., Nanjwade B. K., Sanjiv Singh, Pankaj Purohit, (2010). *Review of the 2-Amino Substituted Benzothiazoles: Different Methods of the Synthesis. Der Pharm. Lett, 2 (1) 347-359.*

Yuping Tong, Jing Fu, Juntao Ma, (2018). *A theoretical investigation about the excited state behavior for 2-(6'-hydroxy-2'-pyridyl) benzimidazole: The water-assisted excited state proton transfer process. J. Chin. Chem. Soc. 65, 822–827.* https://doi.org/10.1002/jccs.201700446.

Fatemeh Niknam, Peyman Hamidizadeh, Masoud Nabavizadeh, Fatemeh Niroomand, Jafar Hoseini, Peter Ford, Mahdi M. Abu-Omar (2019). *Synthesis, structural characterization, and luminescence properties of mono and di-nuclear platinum(II) complexes containing 2-(2-pyridyl)-benzimidazole. Inorg. Chim. Acta 498, 119133.* https://doi.org/10.1016/j.ica.2019.119133.

Xiao-Feng He, Christopher Vogels, Andreas Decken, Stephen Westcott (2004). *Pyridyl benzimidazole, benzoxazole, and benzothiazole platinum complexes. Polyhed. 23, 155–160.* https://doi.org/10.1016/j.poly.2003.09.020.

Frisch M.J., Trucks G.W., Schlegel H.B.,. Scuseria G.E, Robb M.A., Cheeseman J.R., Zakrzewski V.G., Montgomery J.A., Stratmann Jr., R.E., Burant J.C., Dapprich S., Millam J.M., Daniels A.D., Kudin K.N., Strain M.C., Frakas O., Tomasi J., Barone V., Cossi M., Cammi, Mennucci B., Pomelli C., Adamo C., Clifford S., Ochterski J., Petersson G.A., Ayala P.Y., Cui Q., Morokuma K., Malick D.K., Rabuck A.D., Raghavachari K., Foresman J.B., Cioslowski J., Ortiz J.V., Baboul A.G., Stefanov B.B., Liu G., Liashenko A., Piskorz P., Komaromi I., Gomperts R., Martin R.L., Fox D.T., Keith T., Al-Laham M.A., Peng C.Y., Nanayakkara A., Gonzalez C., Challacombe M., Gill P.M.W., Johnson B.G., Chen W., Wong W., Andres J.L., Head-Gordon M., Replogle E.S., Pople J.A.,(2003). *GAUSSIAN 03, Revision B.01, Gaussian, Inc., Pittsburgh, PA.*

Roy Dennington, Todd A. Keith, and John M. Millam, (2016). *Gauss View, Version 6.1, Semichem Inc., Shawnee Mission, KS.*

Jamroz M. H. (2004). *Vibrational Energy Distribution Analysis. VEDA 4 Program, Warsaw.*

El-Rayyes Ali, Yunusa Umar (2005). *Density Functional Theoretical studies on Structures and Vibrational Spectra of Fluorovinyl Silanimines. Can. J. of Anal. Sci. Spect. (CJASS), 50, 175-189.*

El-Rayyes Ali, Maung T. H., (2005). *Excited state Phototautomerization of 8-amino-1-naphthol-3, 6-disulfonate in polar and acidic solutions. Can. J. of Anal. Sci. Spect. (CJASS), 50, 111-118.*

El-Rayyes Ali, Maung T. H. (2004). *Theoretical studies on the structure and hydrogen bonding of 8-amino-1-naphthol and its one water complex. J. Mol. Struct. (Theochem), 681, 9-13.*

El-Rayyes Ali. A. (2003). *Theoretical Studies on the Geometrical Structures and Vibrational Spectra of N-hydroxy-1-vinylsilanimines. J. Mol. Struct. (Theochem), 624, 181-190.*

El-Rayyes Ali. A. (2003). *Structure and vibrational assignments of the various modes of Nitro-, Nitrozo- and Aminosilanimines. J. Mol. Struct. (Theochem)), 634, 289-298.*

Yunusa Umar, El-Rayyes Ali, (2024). *Theoretical investigation of the vibrational and electronic properties of tetraphenylammonium and its boron, aluminum, gallium, carbon, silicon, germane, phosphorus and arsenic analogues. Comp. Theor. Chem, 1231, 114423.*

Evaluation of toxicity of neem essential oil and its nano-emulsion against adult *Oryzaephilus surinamensis* (Coleoptera: Silvanidae)

Fatehia Nasser Gharsan

Department of Biology, Faculty of Science, Al-Baha University, Al-Baha, Saudi Arabia

Abstract: The saw-toothed grain beetle *Oryzaephilus surinamensis* (Coleoptera: Silvanidae) is a widespread warehouse pest that attacks a range of stored food products. Although chemical pesticides are effective to control this beetle, however, these agents are associated with harmful effects on humans and to the environment, indicating the need for safer and ecofriendly alternatives. In the present study, we aimed to compare the efficacy of neem (Azadirachta indica) essential oil and its nano-emulsion in the control of O. surinamensis adults. Neem essential oil was prepared using a steam distillation method, whereas the nano-emulsion was prepared using a non-ionic surfactant. Adults of O. surinamensis were exposed to both preparations, and mortalities were recorded after 24 h. The mean nano-emulsion droplet size was found to be 63.94 nm, and electron microscopy revealed that the nanoparticles occur either as scattered particles or agglomerated in small groups, with size ranging from 6.94 to 13.9 nm. The lethal concentrations of the neem essential oil and its nano-emulsion that cause 50% mortality (LC50) among O. surinamensis adults were 18.2 and 15.7 µL/L of air, respectively, indicating that the LC50 of the nano-emulsion against these beetles was 13.7% lower (p < 0.05) than that of the parent essential oil. Although, beetles were found to be susceptible to both preparations, the higher efficacy of the nano-emulsion as compared to the essential oil indicates that it would be a more promising option for the control of O. surinamensis.

(*) **Corresponding Author**:

Fatehia Nasser Gharsan, Department of Biology, Faculty of Science, Al-Baha University, Al-Baha, Saudi Arabia.

E-mail: fatehia2002@gmail.com

ORCID: 0000-0002-1807-6754

تقييم سمية الزيت العطري للنيم ومستحلب النانو له ضد الطور الكامل لخنفساء الحبوب المنشارية (غمدية الأجنحة: الخنفساء ذات الصدر المنشاري)

د. فتحية ناصر غرسان

الأستاذ المشارك في علم الحشرات

قسم الأحياء، كلية العلوم، جامعة الباحة، المملكة العربية السعودية

مستخلص البحث: خنفساء الحبوب المنشارية تعتبر من آفات المخازن عالمية الانتشار والتي تهاجم مدى واسع من المنتجات والأغذية المخزونة. وبالرغم من فعالية المبيدات الحشرية الكيميائية في مكافحتها إلا أنها ارتبطت بالعديد من الأضرار على الإنسان وبيئته الطبيعية. لذا دعت الحاجة إلى البحث عن بدائل للمبيدات الكيميائية تكون أكثر أماناً وفي ذات الوقت صديقة للبيئة. وتهدف دراستنا الحالية إلى مقارنة فعالية الزيت العطري لنبات النيم مع مستحلب النانو لزيت النيم لمكافحة خنفساء الحبوب المنشارية. وقد تم معاملة الطور البالغ للحشرة وحساب نسب الإماتة بعد 24 ساعة. وكان متوسط حجم قطرات النانو التي تم تحضيرها 63.94 نانومتر، كما تبين من خلال الفحص بالمجهر الإلكتروني أن جسيمات النانو تظهر إما كجسيمات متناثرة أو مجتمعة في مجموعات صغيرة، وبأحجام تتراوح ما بين 6.94 إلى 13.9 نانومتر. دلت النتائج أن تركيز الزيت العطري للنانو ومستحلب النانو له والذي أحدث 50% من الإماتة للطور الكامل للحشرة هو 18.2 و 15.7 ميكرو لتر/لتر هواء على التوالي، وهذا يظهر بأن التركيز المميت لخمسين بالمئة من الحشرات لمستحلب النانو قد كان أقل بنسبة 13.7% عن الزيت العطري للنيم مما يدل على أنه الأكثر فعالية. وبشكل عام أظهرت نتائج المقارنة بين الزيت العطري للنيم و مستحلب النانو للنيم قد يكون له مستقبلاً واعداً في مكافحة خنفساء الحبوب المنشارية.

كلمات مفتاحية: تركيبات نانونية، زيت النيم العطري، مكافحة آفات المنتجات المخزونة.

(*) للمراسلة:

د. فتحيـة ناصـر غرسـان، الأسـتاذ المشـارك فـي علـم الحشـرات، قسـم الأحيـاء، كليـة العلـوم، جامعـة الباحـة، المملكـة العربيـة السـعودية

E-mail: fatehia2002@gmail.com

ORCID: 0000-0002-1807-6754

1. Introduction

Stored grains and other products often become infested with pests that inflict varying degrees of damage, which accordingly reduce product quantity and quality, thereby resulting in considerable economic loss. According to the Food and Agricultural Organization (FAO), approximately 17% of food produced annually is lost, of which 10% is attributable to insect infestation (Stathas et al. 2023). Among pests that affect foodstuffs, the saw-toothed grain beetle *Oryzaephilus surinamensis* (Coleoptera: Silvanidae) causes severe damage to stored food (Gharsan 2022; Kousar et al. 2021), and thus it would be highly desirable to develop effective strategies for controlling and eliminating the damage caused by this beetle. Although in this regard, chemical insecticides are effective to control of *O. surinamensis*, they are associated with a number of potentially harmful effects with respect to human health and the environment (Kim et al. 2017). Consequently, studies are necessary to identify safer and effective alternatives, such as plant extracts, for the control of stored product insects (Ahmed et al. 2021; Alhaithloul et al. 2023; Garay et al. 2020). For example, Gharsan et al. (2018) have reported that onion and lavender oils are particularly effective in combating grain beetles, resulting in mortality rates reaching 100% for onion oil at all concentrations and 90% for lavender oil at a concentration of 4 µL/mL. Additionally, Al Qahtani et al. (2012) established that among the three types of plant powder they assessed, the ginger powder was the most effective in combating grain beetles, with a lethal concentration that causes 50% mortality (LC_{50}) as low as 0.14 mg/g. Neem extracts are among those plant extracts that have widely been used and proven to be effective in the control of insect pests of stored products (Saxena et al, 2018). For example, a study of the efficacy of different neem products (those of leaves, seeds, and bark) against cowpea beetle (*Callosobruchus maculatus*) infestation in bean seeds revealed that powdered seed had the highest protective effect, resulting in the lowest weight loss percentage of bean seeds (0.09%) compared to that in control group (1.16%) (Rajab & Abdullahi 2020). Neem contains a range compound with favorable bioactive properties, among which terpenoids are the most important and can be extracted from different parts of the plant. Additionally, azadirachtin has been identified as one of the most active biological components in neem (da Costa et al. 2014). Moreover, neem contains more than 20 sulfur compounds, which are responsible for its distinctive odor (Lokanadhan et al. 2012). Recently, the efficacy of plant extracts in the control of insects has attracted considerable research attention, notably in the context of the emergence and development of nanotechnology, which has contributed to enhancing the stability of active compounds (Hashem et al. 2020; Melanie et al. 2022; Palermo et al. 2021). In this regard, the toxicities of citronella essential oil and its nano-emulsion against *O. surinamensis* have previously been evaluated, however, to date, there have been no similar studies that have examined the toxicity of neem oil against this beetle. Consequently, in this study, we aimed to evaluate the efficacy of neem essential oil and its nano-emulsion against the adults of *O. surinamensis*.

2. Materials and Methods

2.1 Insect rearing

Saw-toothed grain beetles (*O. surinamensis*) were collected from infected oats and dates from the market of Al-Baha City, Saudi Arabia, and then transferred to the laboratory of the Biology Department, College of Science, University of Al-Baha. The insect was identified by microscopic examination and using identification keys (Vendl et al. 2019). The insects were reared on dry dates within plastic containers (1 L) in an incubator at 27 ± 2°C and 65% ± 5% relative humidity and maintained for several generations to obtain a sensitive population.

2.2 Extraction of neem essential oil

Neem essential oil was extracted from the fresh leaves of neem plants (*Azadirachta indica*, A. Juss, 1830) collected during July 2019 from the Department of Medicinal and Aromatic Plants Research, Institute of Horticulture Research (El-Kanater El-Khairia farm), Egypt. The extracted oil was purified using a steam distillation method. Fresh neem leaves were dried, ground, and 100 gm of powder was placed in 300 ml of water and then distilled using a Clevenger apparatus for 3 hours. (Wu et al. 2019).

2.3 Preparation of a neem nano-emulsion

A nano-emulsion of the neem extract was prepared by mixing 10 mL of neem essential oil with 5 mL of a non-ionic surfactant (Tween 80), followed by slow stirring until a homogeneous mixture had formed. Thereafter, the mixture was diluted with 85 mL of water to obtain final volume of 100 mL, followed by continuous stirring for 30 min using a magnetic stirrer to ensure adequate dispersion and complete incorporation. The mixture thus obtained was divided into two portions, both of which were sonicated at 700 W using a SONOPULS HD 2200 ultrasonicator (Bandelin, Germany): one portion for 15 min and the other for 1.5 h. The size of the particles in each portion of the 10% neem nano-emulsion were determined using a hydrodynamic light scattering analyzer (DLS) following storage for 90 d at 27°C (Hassanin et al. 2017).

2.4 Determination of nano-emulsion droplet size

The size of the neem nano-emulsion droplets was measured at 27 °C using a Zetasizer Nano ZS particle sizer (Malvern Instruments, UK). Briefly, prior to measurement, 30 μL of the nano-emulsion was diluted with 3 mL of water at 25 °C. Molecule size information is presented as the mean Z-normal of three independent batches of nano-emulsions (Hassanin et al. 2017).

2.5 Transmission electron microscopy

The samples for transmission electron *m*icroscopy observation were prepared initially by pipetting a 20-μL diluted sample onto a 200-mesh copper specimen grid coated in film, followed by incubation for 10 min, with subsequent blotting of excess liquid. Thereafter, the grid was stained with one drop of 3% phosphotungstic acid and allowed to dry for 3 min. Finally, the dried coated grid was observed using a Tecnai G20 Super TWIN double-tilt transmission electron microscope (FEI, Netherlands) operated at 200 kV (Hassanin et al. 2017)

2.6 Fumigant toxicity

To assess the toxicity of neem essential oil and its nano-emulsion against *O. surinamensis*, 10 adult insects (2 weeks old) were placed in 1-L plastic containers, in which were suspended filter papers (1 cm × 1 cm) soaked with graded concentrations of neem essential oil as well as its nano-emulsion (10, 15, 20, and 25 μL/L). Control group insects were maintained in containers in which untreated filter papers were suspended. The insects were exposed to the test materials for 24 h, after which the number of dead insects was counted under a microscope. The experiments were performed under laboratory conditions at 27 ± 2°C with 65% ± 5% relative humidity (Gharsan et al. 2022; Malacrinò et al. 2016).

2.7 Statistical Analysis

The percentage mortality was calculated and corrected according to the formula proposed by Abbott (1925), as follow:

Percentage mortality of treated insects = (percentage of dead insects in the control/total number of tested insects) × 100

After calculation of the percentage mortalities, the toxicity data were analyzed to determine the lethal concentration to 50% of the insects (LC_{50}; Ldp line) using probit analysis (Finney 1952). Significant differences between the groups were determined by one-way ANOVA, followed by Tukey's honest significant difference (HSD) tests, and statistical significance was set at $p < 0.05$. All statistical analyses were performed using SPSS (USA-based IBM Corp.).

3. Results

3.1 Droplet size and polydispersity of the neem nano-emulsion

The mean droplet diameter of the prepared neem nano-emulsion was 63.94 nm (Fig. 1), and the value of the polydispersity index, an indicator of polydispersity and a measure of the regularity and stability of droplet size, of this preparation was found to be 0.364.
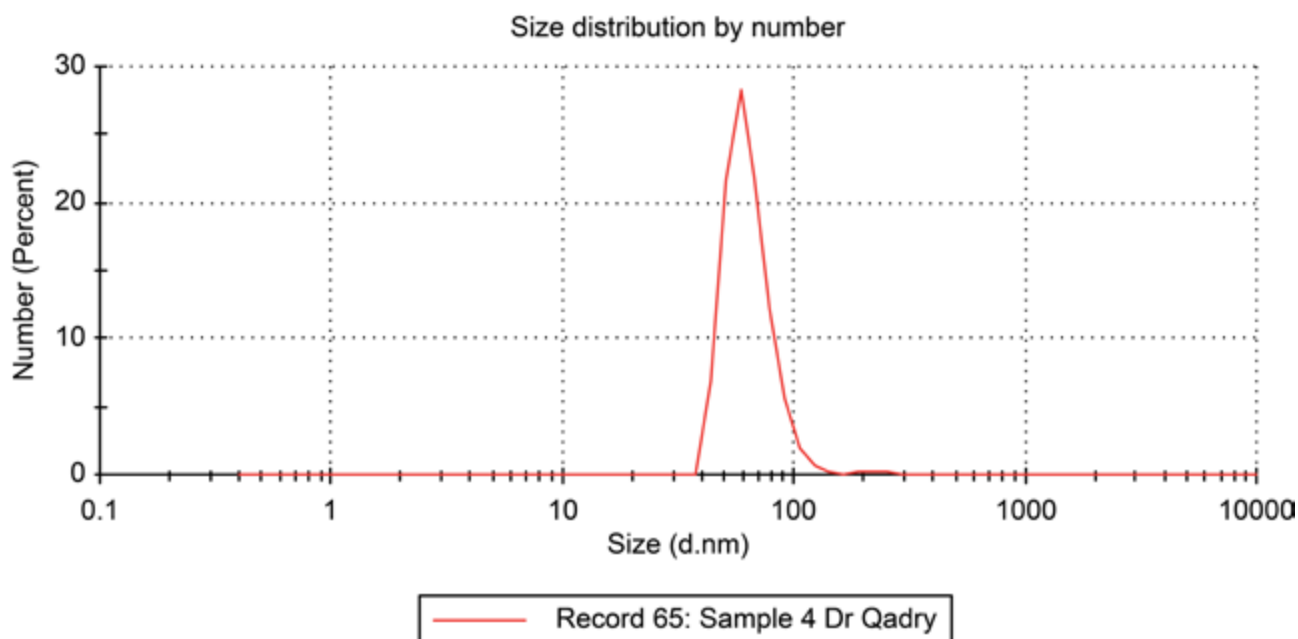

Figure 1. Mean droplet size (nm) of neem nano-emulsion.

3.2 Characteristics of neem nano-emulsions

The shape and size of the nanoparticles, which were determined from transmission electron micrographs, revealed that the particles are dark and spherical, and they appeared either as single scattered particles or in small clusters ranging in size from 6.94 to 13.9 nm (Fig. 2).
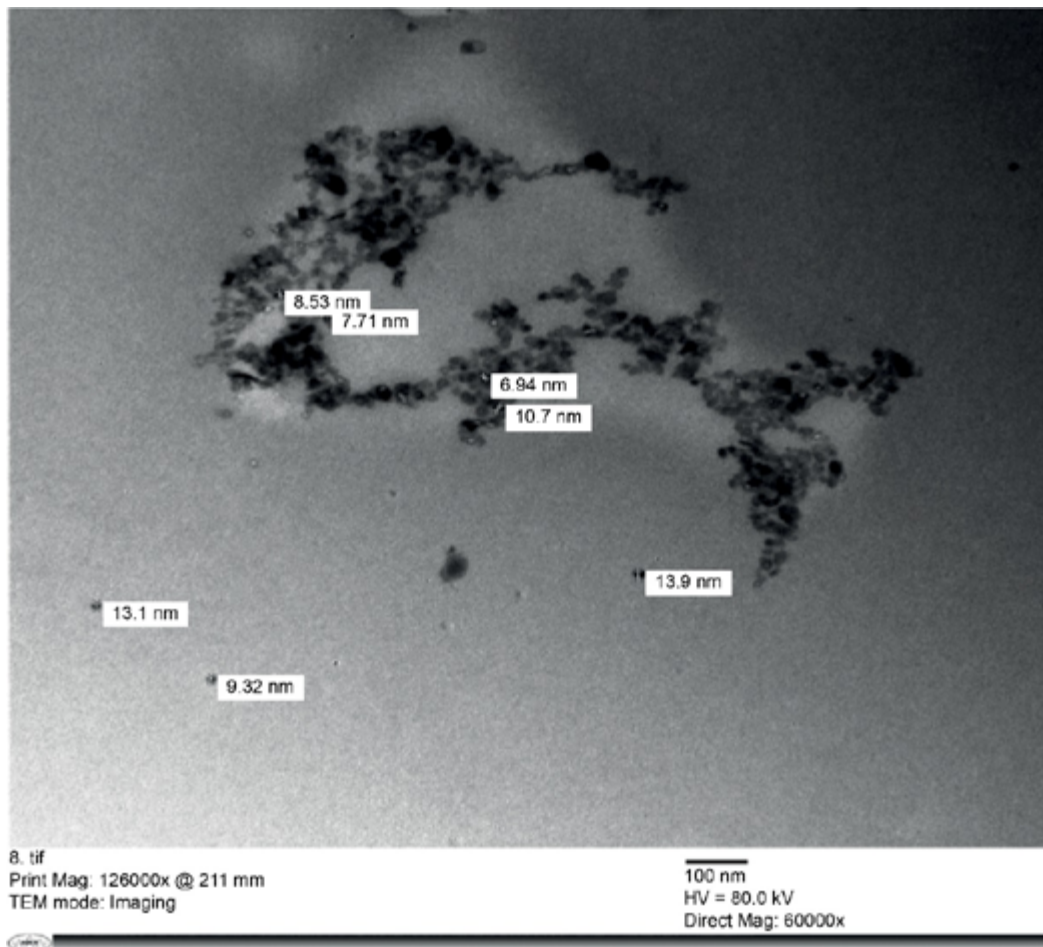

Figure 2. Representative transmission election microscopy image of neem nano-emulsion

3.3 Toxicity of neem essential oil against *O. surinamensis* adults

The essential oil of neem showed a concentration-dependent increase in toxicity against *O. surinamensis* adults, with mean mortality rates of 8%, 28%, 57%, and 81% , being recorded at concentrations of 10, 15, 20, and 25 µL/L, respectively (Table 1 and Fig. 3). On the basis of these findings, the LC_{50} and LC_{95} values of neem essential oil against *O. surinamensis* adults were calculated as 18.2 and 35.5 µL/L, respectively.
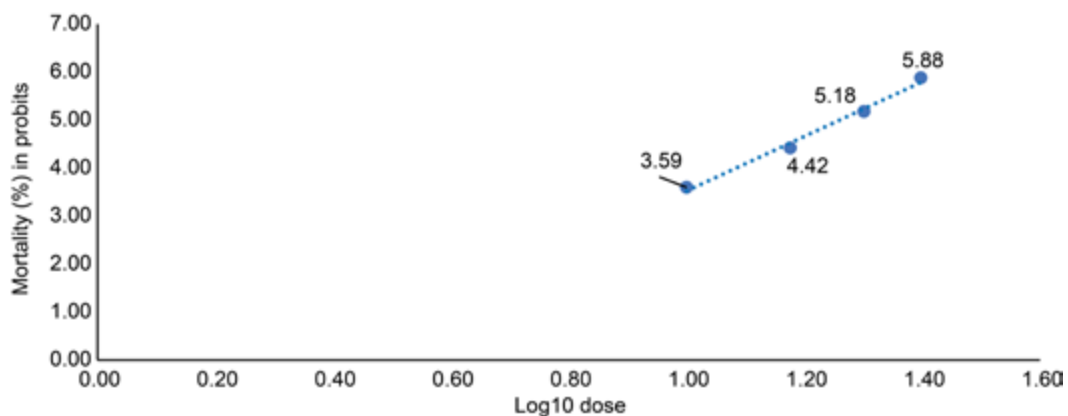

Figure 3. Regression line of Log concentration-mortality of neem essential oil on *Oryzaephilus surinamensis* adults.

46

Table 1 Toxicity of neem essential oil and neem nano-emulsion against *Oryzaephilus surinamensis* adults

	Conc. μL/L of air	Mean toxicity (percentage)	Sig.	LC50	LC95	Slope	Sig.
Essential oil of neem	10	8	0.782	18.2a*	35.5	5.7	0.02
	15	28					
	20	57					
	25	81					
	Control	0					
Neem nano-emulsion	10	3.3	0.031	15.7b	22.6	10.6	
	15	25					
	20	91.6					
	25	100					
	Control	0					

* Different letters following values in the same column indicate statistically significant differences at the p < 0.05 level.

3.4 Toxicity of neem nano-emulsion against *O. surinamensis* adults

Consistent with the parent oil, the neem nano-emulsion was found to show a concentration-dependent increase in toxicity against the insects, with mean mortalities ranging from 3.3% to 100% at concentrations from 10 to 25 μL/L of air (Table 1 and Fig. 4), and an LC_{50} value of 15.7 µl/L.
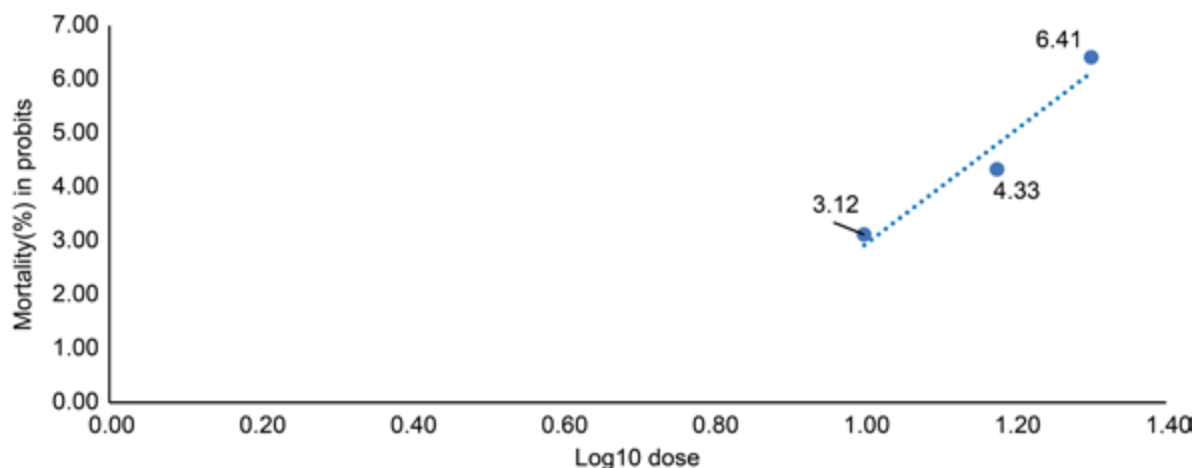
Figure 4. Regression line of Log concentration-mortality of neem nano-emulsion on *Oryzaephilus surinamensis* adults.

4. Discussion

In this study, it has been observed that the neem essential oil was effective in eliminating *O. surinamensis*, which is consistent with the findings of previous studies that has evaluated the exterminatory effects of neem against insect pests of stored products (Mantzoukas et al. 2020; Muhammad & Kashere 2020; Onu et al. 2015). Neem contains range of active substances, which are presumed to contribute to the efficacy of neem extracts in controlling insects, among which, the limonoids present in neem are believed to be responsible for its insecticidal properties. Although azadirachtin has been identified as the most active compound in neem, other limonoids may also contribute in enhancing its activity and efficacy, as well as to preventing insect resistance (Iqbal et al. 2021). Compared with that of the neem oil, we noted a 13.7% reduction in the LC_{50} of the nano-emulsion against *O. surinamensis* adults, thereby indicating that the nano-emulsion was more effective than its parent essential oil in controlling these beetles. These results are consistent with previous findings indicating that the conversion of essential oils to nano-emulsions enhances their efficacy in eliminating

insects (Giunti et al. 2019; Gharsan et al. 2022; Manjesh et al. 2022; Palermo et al. 2021; Sabbour 2020). For example, da Costa et al. (2014) found that the mortality of *Zabrotes subfasciatus* increased when exposed to nanocomposites of neem extract, and also noted that the compounds were more stable than the parent extract.

In the present study, we obtained a value of 63.94 nm for the mean droplet size of the prepared neem nano-emulsion, which is within the 20–200 nm droplet size range, considered to be suitable for a good nano-emulsion (Ibrahim 2020; Ostertag et al. 2012). The neem nano-emulsion was prepared using a surfactant (Tween 80), which has been reported to ensure the stability of emulsions of essential oils (Mansouri et al. 2021). For example, Ali et al. (2017) have confirmed that the use of Tween 80 in combination with high-energy sonication promoted the formation of a stable and durable nano-emulsion. In addition, to enhance the stability of plant extracts, there are certain other advantages also associated with the use of nano-emulsions in the field of pest control, including an increased solubility of the active

constituents and enhanced wettability during application (Mustafa & Hussein 2020). Moreover, the small size of the nanoparticles comprising nano-emulsions facilitates active constituent penetration through the insect cuticle, thereby enhancing their ability to eliminate insects (Margulis-Goshen & Magdassi 2013). However, one of the limitations of the present study is that all experiments were conducted under laboratory conditions, and consequently, it is necessary to further validate our findings under actual storage conditions.

Conclusively, the findings of this study will make a valuable contribution to the field of pest control, and in particular control of the pests of stored products, as plant extract nanoparticles have shown to possess a number of important advantages. Moreover, the continued application of nanotechnology will no doubt contribute to the discovery of other effective compounds for control of the insect pests of stored products.

5. Conclusions

In this study, we compared the pesticidal activities of a neem essential oil and its nano-emulsion against the adults of *O. surinamensis*. The conversion of neem essential oil to a nano-emulsion was found to significantly enhance its toxic effects against *O. surinamensis*. Although the efficacy of natural plant products in controlling insects is often attributable to the action of their active compounds, these plants products and their bioactive compounds tend to be unstable and are susceptible to deactivation or degradation by multiple factors. However, converting compounds of plant origin to a corresponding nano form can enhance their stability, thereby making them more promising candidates for the control of insect pests. Moreover, nano-emulsions can be incorporated as a complementary component of integrated pest management programs.

6. Acknowledgements

7. References

Abbott, W. S. (1925). A method of computing the effectiveness of an insecticide. J. *econ. Entomol*, 18(2), 265-267.

Ahmed, N., Alam, M., Saeed, M., Ullah, H., Iqbal, T., Al-Mutairi, K. A., ... & Salman, M. (2021). Botanical insecticides are a non-toxic alternative to conventional pesticides in the control of insects and pests. *Global decline of insects*, 1-19.

Al Qahtani, A. M., Al-Dhafar, Z. M., & Rady, M. H. (2012). Insecticidal and biochemical effect of some dried plants against *Oryzaephilus surinamensis* (Coleoptera-Silvanidae). *The Journal of Basic & Applied Zoology*, 65(1), 88-93.

Alhaithloul, H. A., Alqahtani, M. M., Abdein, M. A., Ahmed, M. A., Hesham, A. E. L., Aljameeli, M. M., ... & El-Amier, Y. A. (2023). Rosemary and neem methanolic extract: antioxidant, cytotoxic, and larvicidal activities supported by chemical composition and *molecular docking simulations. Frontiers in Plant Science*, 14, 1155698.

Ali, E. O. M., Shakil, N. A., Rana, V. S., Sarkar, D. J., Majumder, S., Kaushik, P., ... & Kumar, J. (2017). Antifungal activity of nano emulsions of neem and citronella oils against phytopathogenic fungi, Rhizoctonia solani and Sclerotium rolfsii. *Industrial crops and products*, 108, 379-387.

da Costa, J. T., Forim, M. R., Costa, E. S., De Souza, J. R., Mondego, J. M., & Junior, A. L. B. (2014). Effects of different formulations of neem oil-based products on control Zabrotes subfasciatus (Boheman, 1833) (Coleoptera: Bruchidae) on beans. *Journal of Stored Products Research*, 56, 49-53.

Finney, D.J. (1952). Probit Analysis (2nd Ed), *Cambridge University Press*, New York, 388-390.

Garay, J., Brennan, T., and Bon, D, (2020). Review: Essential oils a viable pest control alternative. International Journal of *Ecotoxicology and Ecobiology*, 5, 13-22.

Gharsan, F., Jubara, N., Alghamdi, L., Almakady, Z., & Basndwh, E. (2018). Toxicity of five plant oils to adult Tribolium castaneum (Coleoptera: Tenebrionidae) and *Oryzaephilus surinamensis* (Coleoptera: Silvanidae). *Florida Entomologist*, 592-596.

Gharsan, F. N., Kamel, W. M., Alghamdi, T. S., Alghamdi, A. A., Althagafi, A. O., Aljassim, F. J., & Al-Ghamdi, S. N. (2022). Toxicity of citronella essential oil and its nanoemulsion against the saw-toothed grain beetle *Oryzaephilus surinamensis* (Coleoptera: Silvanidae). *Industrial crops and products*, 184, 115024.

Gharsan, F. N. (2022). Estimating the Susceptibility of Four Wheat Cultivars to the Saw-Toothed Grain Beetle *Oryzaephilus surinamensis* (L.) (Coleoptera: Silvanidae). *International Journal of Food Science*, 2022.

Giunti, G., Palermo, D., Laudani, F., Algeri, G. M., Campolo, O., & Palmeri, V. (2019). Repellence and acute toxicity of a nano-emulsion of sweet orange essential oil toward two major stored grain insect pests. *Industrial Crops and Products*, 142, 111869.

Hashem, A. S., Ramadan, M. M., Abdel-Hady, A. A., Sut, S., Maggi, F., & Dall'Acqua, S. (2020). Pimpinella anisum essential oil nanoemulsion toxicity against Tribolium castaneum? Shedding light on its interactions with aspartate aminotransferase and alanine aminotransferase by molecular docking. *Molecules*, 25(20), 4841.

Hassanin, M. M., Halawa, A. E., & Ali, A. A. A. (2017). Evaluation of the activity of thyme essential oil nanoemulsion against Sclerotinia rot of fennel. *Egyptian Journal of Agricultural Research*, 95(3), 1037-1050.

Ibrahim, S. S. (2020). Essential oil nanoformulations as a novel method for insect pest control in horticulture. *Horticultural crops*, 195-209.

Iqbal, T., Ahmed, N., Shahjeer, K., Ahmed, S., Al-Mutairi, K. A., Khater, H. F., & Ali, R. F. (2021). Botanical insecticides and their potential as anti-insect/pests: Are they successful against insects and pests?

Kim, K. H., Kabir, E., & Jahan, S. A. (2017). Exposure to pesticides and the associated human health effects. *Science of the total environment*, 575, 525-535.

Kousar, T., Zaib-un-Nisa Memon, H. A., Sahito, W. M. M., Jatoi, F. A., & Shah, Z. H. (2021). 1. Biology, morphology, and varietal distribution of Saw-toothed grain beetle, *Oryzaephilus surinamensis* (L) on date palm dry and semi-dry dates at district: Khairpur, Sindh-Pakistan. *Pure and Applied Biology* (PAB), 10(3), 539-548.

Lokanadhan, S., Muthukrishnan, P., & Jeyaraman, S, (2012). Neem products and their agricultural applications. *Journal of Biopesticides* 5: 72.

Malacrinò, A., Campolo, O., Laudani, F., & Palmeri, V. (2016). Fumigant and repellent activity of limonene enantiomers against Tribolium confusum du Val. *Neotropical entomology*, 45(5), 597-603.

Manjesh, K., Kundu, A., Dutta, A., Saha, S., & Neelakanthaiah, B. S. (2022). Bio-insecticidal nanoemulsions of essential oil and lipid-soluble fractions of Pogostemon cablin. *Frontiers in Plant Science*, 13, 874221.

Mansouri, S., Pajohi-Alamoti, M., Aghajani, N., Bazargani-Gilani, B., & Nourian, A. (2021). Stability and antibacterial activity of Thymus daenensis L. essential oil nanoemulsion in mayonnaise. *Journal of the Science of Food and Agriculture*, 101(9), 3880-3888.

Mantzoukas, S., Ntoukas, A., Lagogiannis, I., Kalyvas, N., Eliopoulos, P., & Poulas, K. (2020). Larvicidal action of cannabidiol oil and neem oil against three stored product insect pests: effect on survival time and in progeny. *Biology*, 9(10), 321.

Margulis-Goshen, K., & Magdassi, S. (2013). Nanotechnology: an advanced approach to the development of potent insecticides. *Advanced technologies for managing insect pests*, 295-314.

Melanie, M., Miranti, M., Kasmara, H., Malini, D. M., Husodo, T., Panatarani, C., ... & Hermawan, W. (2022). Nanotechnology-based bioactive antifeedant for plant protection. *Nanomaterials*, 12(4), 630.

Muhammad, A., & Kashere, M. A. (2020). Neem, Azadirachta indica L. (A. Juss): An eco-friendly botanical insecticide for managing farmers insect pest problems-a review. *FUDMA Journal of Sciences*, 4(4), 484-491.

Mustafa, I. F., & Hussein, M. Z. (2020). Synthesis and technology of nanoemulsion-based pesticide formulation. *Nanomaterials*, 10(8), 1608.

Onu, F. M., Ogu, E., & Ikehi, M. E. (2015). Use of Neem and Garlic Dried Plant Powders for Controlling some Stored Grains Pests. *Egyptian Journal of Biological Pest Control*, 25(2).

Ostertag, F., Weiss, J., & McClements, D. J. (2012). Low-energy formation of edible nanoemulsions: factors influencing droplet size produced by emulsion phase inversion. *Journal of colloid and interface science*, 388(1), 95-102.

Palermo, D., Giunti, G., Laudani, F., Palmeri, V., & Campolo, O. (2021). Essential oil-based nano-biopesticides: Formulation and bioactivity against the confused flour beetle Tribolium confusum. *Sustainability*, 13(17), 9746.

Rajab, Y. S., & Abdullahi, U. (2020). Efficacy of Various Neem Products in Control of Storage Pests (Callosobruchus maculatus) of Cowpea (Vigna unguiculata). *IOSR Journal of Agriculture and Veterinary Science* (IOSR-JAVS), 13(3), 23-26.

Sabbour, M. M. A. (2020). Efficacy of nano-formulated certain essential oils on the red flour beetle Tribolium castaneum and confused flour beetle, Tribolium confusum (Coleoptera: Tenebrionidae) under laboratory and storage conditions. *Bulletin of the National Research Centre*, 44, 1-7.

Saxena, R. C., Jilani, G., & Kareem, A. A. (2018). Effects of neem on stored grain insects. *In Focus on phytochemical pesticides* (pp. 97-112). CRC Press.

Stathas, I. G., Sakellaridis, A. C., Papadelli, M., Kapolos, J., Papadimitriou, K., & Stathas, G. J. (2023). The Effects of Insect Infestation on Stored Agricultural Products and the Quality of Food. *Foods*, 12(10), 2046.

Vendl, T., Stejskal, V., & Aulicky, R. (2019). Comparative tarsal morphology of two secondary stored product beetle pests, *Oryzaephilus surinamensis* (L.) and *Cryptolestes ferrugineus* (Stephens), that vary in their climbing ability on smooth surfaces. *Journal of stored products research*, 82, 116-122.

Wu, H., Li, J., Jia, Y., Xiao, Z., Li, P., Xie, Y., ... & Li, C. (2019). Essential oil extracted from Cymbopogon citronella leaves by supercritical carbon dioxide: antioxidant and antimicrobial activities. *Journal of Analytical Methods in Chemistry*, 2019.

الأبحاث باللغة الإنجليزية

المحتويات

الأبحـاث باللغـة الإنجليزية

شروط النشر

أولاً: ضوابط النص المقدم للنشر

1) ألا تزيد صفحاته عن (35) صفحة من القطع العادي (A4).

2) أن يحتوي على عنوان البحث وملخصه باللغتين العربية والإنجليزية في صفحةٍ واحدة، بحيث لا يزيد عن (250) كلمة للملخص، وأن يتضمن البحث كلمات مفتاحيةٍ دالة على التخصص الدقيق للبحثِ باللغتَين، بحيث لا يتجاوز عددها (6) كلمات، توضع بعد نهاية كل ملخص.

3) أن يذكر اسم المؤلف وجهة عمله بعد عنوان البحث مباشرة باللغتين العربية والإنجليزية.

4) أن تقدم البحوث العربية مطبوعة بخط (Simplified Arabic)، بحجم (14) للنصوص في المتن، وبالخط نفسه بحجم (12) للهوامش.

5) أن تقدم البحوث الإنجليزية مطبوعة بخط (Times New Roman) بحجم (12) للنصوص في المتن، وبالخط نفسه بحجم (9) للهوامش.

6) كتابة البحث على وجه واحد من الصفحة، مع ترك مسافة سطر واحد بين السطور، وتكون الحواشي 2.5 سم على الجوانب الأربعة للصفحة، بما يعادل 1.00 إنش (بوصة).

7) التزام الترتيب الموضوعي الآتي:

المقدمـــة: تكون دالة على موضوع البحث، والهدف منه، ومنسجمة مع ما يَرِدُ في البحث من معلومات وأفكار وحقائق علمية، كما تشير باختصار إلى مشكلة البحث، وأهمية الدراسات السابقة.

العـرض: يتضمن التفاصيل الأساسية لمنهجية البحث، والأدوات والطرق التي تخدم الهدف، وترتب المعلومات حسب أولويتها.

النتائج والمناقشة: يجب أن تكون واضحة موجزة، مع بيان دلالاتها دون تكرار.

الخاتمة: تتضمن تلخيصًا موجزًا للموضوع، وما توصل إليه الباحث من نتائجٍ، مع ذكر التوصيات والمقترحات.

8) أن تدرج الرسوم البيانية والأشكال التوضيحية في النص، وترقم ترقيماً متسلسلاً، وتكتب أسماؤها والملاحظات التوضيحية أسفلها.

9) أن تدرج الجداول في النص، وترقم ترقيماً متسلسلاً، وتكتب أسماؤها أعلاها، وأما الملاحظات التوضيحية فتكتب أسفل الجدول.

10) ألا توضع الهوامش أسفل الصفحة إلا عند الضرورة فقط، ويشار إليها برقم أو نجمة، ويكون الخط فيها بحجم (12) للعربي و (9) للإنجليزي.

11) لا تنشر المجلة أدوات البحث والقياس، وتقوم بحذفها عند طباعة المجلة.

12) أن يُراعى في منهج توثيق المصـادر والمراجـع داخل النص نظام (APA)، وهـو نظام يعتمـد ذكر الاسم والتاريخ (name/year) داخل المتن، ولا يقبل نظام ترقيم المراجع داخل النص مع وضع الحاشية أسفل الصفحة، وتوضع المصادر والمراجع داخل المتن بين قوسين حسب الأمثلة الآتية: يذكر اسم عائلة المؤلف متبوعا بفاصلة، فسنة النشر، مثلا: (مجاهد، 1988م). وفي حالة الاقتباس المباشر يضاف رقم الصفحة مباشرة بعد تاريخ النشر مثلا: (خيري، 1985م، ص:33). أما إذا كان للمصدر مؤلفان فيذكران مع اتباع الخطوات السابقة مثلا: (الفالح وعياش، 1424هـ). وفي حالة وجود أكثر من مؤلفين فتذكر أسماء عوائلهم أول مرة، مثلا: (مجاهد والعودات والشيخ، 1408هـ)، وإذا تكرر الاقتباس من المصدر نفسه فيشار إلى اسم عائلة المؤلف الأول فقط، ويكتب بعده وآخرون مثل: (مجاهد وآخرون، 1408هـ)، على أن تكتب معلومات النشر كاملة في قائمة المصادر والمراجع.

13) تخرج الأحاديث والآثار على النحو الآتي:
(صحيح البخاري، ج:1، ص: 5، رقم الحديث 511).

14) توضع قائمة المصادر والمراجع في نهاية البحث مرتبة ترتيباً هجائياً حسب اسم العائلة، ووفق نظام جمعية علم النفس الأمريكية (APA) الإصدار السادس، وبحجم (12) للعربي و(9) للإنجليزي، وترتب البيانات الببليوغرافية على النحو الآتي:

- **الاقتباس من كتاب لمؤلف واحد:**
الخوجلي، أحمد. (2004م). *مبادئ فيزياء الجوامد*. الخرطوم، السودان: عزة للنشر والتوزيع.

- **الاقتباس من كتاب لأكثر من مؤلف:**

نيوباي، تيموثي؛ ستيبيتش، دونالد؛ راس، جيمس. (1434هـ/2013م). *التقنية التعليمية للتعليم والتعلم*. الرياض، المملكة العربية السعودية: دار جامعة الملك سعود للنشر.

- **الاقتباس من دورية:**

النافع، عبداللطيف حمود. (1427هـ). أثر قيادة السيارات خارج الطرق المعبدة في الغطاء النباتي بالمنتزهات البرية: دراسة في حماية البيئة، في وسط المملكة العربية السعودية. *المجلة السعودية في علوم الحياة، 14*(1)، 53-72.

- **الاقتباس من رسالة ماجستير أو دكتوراه:**

القاضي، إيمان عبدالله. (1429هـ). *النباتات الطبيعية للبيئة الساحلية بين رأسي تنورة والملوح بالمنطقة الشرقية: دراسة في الجغرافيا النباتية وحماية البيئة*. رسالة دكتوراه غير منشورة، كلية الآداب للبنات، الدمام، المملكة العربية السعودية: جامعة الملك فيصل.

- **الاقتباس من الشبكة العنكبوتية (الإنترنت):**

  – **الاقتباس من كتاب:**

المزروعــــــــي، م.ر. و المدني، م.ف. (2010م). *تقييــم الأداء فـي مؤسســات التعليــم العالــي*. المعــرِّف الرقمــي (x-xxxxxxxx-xxxx/DOI:10.xxxx)، أو برتوكـول نقـل النصــوص التشــعبي (...http://www)، أو الرقــم المعيــاري الدولــي للكتاب (0-00 -000000- 0 : ISBN)

  – **الاقتباس من مقالة في دورية:**

المدني، م.ف. (2014). مفهوم الحــوار في تقريب وجهات النظر. *المجلة البريطانية لتكنولوجيا التعليم، 11*(6)، 225-260. المعرِّف الرقمي (x-xxxxxxxx-xxxx/DOI:10.xxxx) أو برتوكول نقل النصوص التشعبي (//http: onlinelibrary.wiley.com/journal/10.1111)، أو الرقم المعياري التسلسلي الدولي للمجلة (1467 - ISSN: 8535).

(15) يلتزم الباحث بترجمة (أو رومنة) أسماء المصادر والمراجع العربية إلى اللغة الإنجليزية في قائمة المصادر والمراجع. وعلى سبيل المثال:

الجبر، سليمان. (1991م). تقويم طرق تدريس الجغرافيا ومدى اختلافها باختلاف خبرات المدرسين وجنسياتهم وتخصصاتهم في المرحلة المتوسطة بالمملكة العربية السعودية. *مجلة جامعة الملك سعود- العلوم التربوية، 3*(1)، 143-170.

Al-Gabr, S. (1991). The Evaluation of Geography Instruction and the Variety of its Teaching Concerning the Experience, Nationality, and the Field of Study in Intermediate Schools in Saudi Arabia *(in Arabic). Journal of King Saud University- Educational Sciences, 3*(1), 143-170.

(16) تستخدم الأرقام العربية الأصلية (0، 1، 2، 3، ...) في البحث.

(17) تؤول جميع حقوق النشر للمجلة في حال إرسال البحث للتحكيم وقبوله للنشر.

ثانياً: الأشياء المطلوب تسليمها

1) نسخة إلكترونية من البحث بصيغتي (WORD) و (PDF)، وترسلان على البريد الإلكتروني الآتي:

s.journal@nbu.edu.sa

2) السيرة الذاتية للباحث، متضمنة اسمه باللغتين العربية والإنجليزية، وعنوان البريد الإلكتروني الحالي، ورتبته العلمية.

3) تعبئة النماذج الآتية:

أ - نموذج طلب نشر بحث في المجلة.

ب - نموذج تعهد بأن البحث غير منشور أو مقدم للنشر في مكان آخر.

ثالثاً: تنبيهات عامة

1) أصول البحث التي تصل إلى المجلة لا تردّ سواء أَنُشِرَتْ أم لم تنشر.

2) الآراء الواردة في البحوث المنشورة تعبر عن وجهة نظر أصحابها.

مجلـة الشمــال
للعلوم الأساسية والتطبيقية
(JNBAS)

دورية علمية محكمة

مجلة الشمال للعلوم الأساسية والتطبيقية (JNBAS)

التعريف بالمجلة

تعنى المجلة بنشر البحوث والدراسات العلمية الأصيلة في مجال العلوم الأساسية والتطبيقية، باللغتين العربية والإنجليزية، كما تهتم بنشر جميع ما له علاقة بعرض الكتب ومراجعتها أو ترجمتها، وملخصات الرسائل العلمية، وتقارير المؤتمرات والندوات العلمية، وتصدر مرتين في السنة (مايو ـ نوفمبر).

الرؤية

الريادة في نشر البحوث العلمية المحكمة، وتصنيف المجلة ضمن أشهر الدوريات العلمية العالمية.

الرسالة

نشر البحوث العلمية المحكمة في مجال العلوم الأساسية والتطبيقية وفق معايير عالمية متميزة.

أهداف المجلة

1) أن تكون المجلة مرجعًا علميًا للباحثين في العلوم الأساسية والتطبيقية.
2) تلبية حاجة الباحثين إلى نشر بحوثهم العلمية، وإبراز مجهوداتهم البحثية على المستويات المحلية والإقليمية والعالمية.
3) المشاركة في بناء مجتمع المعرفة بنشر البحوث الرصينة التي تؤدي إلى تنمية المجتمع.
4) تغطية أعمال المؤتمرات العلمية المحكمة.

شروط قبول البحث

1) الأصالة والابتكار وسلامة المنهج والاتجاه.
2) الالتزام بالمناهج والأدوات والوسائل العلمية المتبعة في مجاله.
3) الدقة في التوثيق والمصادر والمراجع والتخريج.
4) سلامة اللغة.
5) أن يكون البحث غير منشور أو مقدم للنشر في أي مكان آخر.
6) أن يكون البحث المستل من الرسائل العلمية غير منشور أو مقدم للنشر، وأن يشير الباحث إلى أنه مستلٌ.

2007 - 1428

جامعة الحدود الشمالية
NORTHERN BORDER UNIVERSITY

المملكة العربيــة السعوديــة

مجلـة الشمـال

للعلــوم

الأساسية والتطبيقية

دورية علمية محكمة

جامعة الحدود الشمالية

www.nbu.edu.sa